Author

Philip Fisk Ong

Title

Early Rotation in the Pennsylvania Salient (US Appalachians): Evidence from Calcite-Twinning Analysis

Submitted for Publication in:

Tectonophysics

in lieu of thesis in partial fulfillment
of the requirements for the degree of
Master of Science in Geology
Department of Geological Sciences
The University of Michigan

Accepted by:

Signature	Name	Date
	Ben A. van der Pluijm	Nov 1, 2004
Rob Van der Voo	Rob van der Voo	Nov. 1, 2004
Joel D. Blum (Department Chair)	Joel D. Blum	Nov 4, 2004

I hereby grant the University of Michigan, its heirs and assigns, the non-exclusive right to reproduce and distribute single copies of my thesis, in whole or in part, in any format. I represent and warrant to the University of Michigan that the thesis is an original work, does not infringe or violate any rights of others, and that I make these grants as the sole owner of the rights to my thesis. I understand that I will not receive royalties for any reproduction of this thesis.

- [x] Permission granted.
- [ ] Permission granted to copy after: ______ (Date)
- [ ] Permission declined.

Author Signature

Philip Fisk Ong

Early rotation in the Pennsylvania Salient

(US Appalachians);

Evidence from calcite-twinning analysis

Abstract

Calcite twinning analysis of Paleozoic limestones from 42 sites reveals that the change in regional strike along the frontal edge of the Pennsylvania salient is accompanied by an equal magnitude rotation of paleostress directions of about 60 degrees. The rotation, recorded by results from 22 reliable sites, shows no discernable difference between sites of Cambro-Ordovician and Siluro-Devonian age and is not present in foreland sites. Scatter in the data attributed to grain-scale rotations and compaction overprinting, reduced by data cleaning methods as well as by the use of more advanced contouring and data averaging methods, reveal a main layer-parallel north-northwesterly oriented stress field as well as a subordinate secondary transpressional event, sinistral in the southern part of the salient. Comparison of paleostress directions within the rotated arc reveal minor rotations in the southwest region of the salient with the bulk of rotation accommodated by the northern salient limb. We propose a model in which these rotations result mostly from dextral transpression of thrust sheets inpinged on a northerly-bounding, rigid cratonic block. This created a structural anisotropy that guided the post-rotational formation of folds in place, producing the current configuration of the salient. The formation of curved but unrotated folds is responsible for both the lack of tangential extension and compression as well as for the divergent evolution of kinematic directions described by previous workers.

Introduction

A feature of most, if not all, fold-thrust belts in the world is the presence of curved segments, with a degree of curvature that may range from tens of degrees to as much as 180°. Orogenic curvature was already noted a century ago (Hobbs, 1914) and in the mid-1950's Carey introduced the term 'orocline' to describe this common geometry (Carey, 1955). Originally, orocline was used to describe a straight belt that later became curved (secondary curvature), but the term is used today to describe both originally curved segments (primary curvature) as well as secondary curvature of belts (Eldredge et al., 1985; Marshak, 1988; Hindle and Burkhard, 1999). Current interpretations for curved belts range from primary curvature, progressive rotational displacements, secondary curvature, or combinations, based on kinematic, paleomagnetic and modeling studies (e.g., Spraggins and Dunne, 2002; Sussman et al., 2004). The origin of secondary curvature has been variably attributed to indentation by a microplate or to changing stress fields (e.g., Weil et al, 2000).

The Pennsylvania salient, one of the more striking features of the Appalachian mountain belt in map view, accomodates the change in orientation of structural features from a south-southwesterly direction in the central Appalachians to an easterly direction farther north near the New York-Pennsylvania border (Figure 1). The evolution of the Pennsylvania salient remains a topic of active discussion (e.g. Fairview, in press; Wise, in press), in large part due to seemingly conflicting kinematic and paleomagnetic data on the curvature of the belt. Paleomagnetic results indicate a prefolding rotation of 20-30° between inner segments of the salient limbs, based on multiple magnetizations (Kent, 1988; Stamatakos and Hirt, 1994; Stamatakos et al., 1996). Kinematic data show a consistent, parallel early shortening direction that diverges clockwise in the northern and counter-clockwise in the southern salient limbs over time (Nickelsen, 1979; Geiser and Engelder, 1983; Gray and Mitra, 1993; Zhou and Jacobi, 1997; Younes and Engelder, 1997), in contrast to the pure-bending model typically associated with oroclinal evolution. Conflicting paleomagnetic and kinematic scenarios have prompted new hypotheses (Gray and Stamatakos, 1997; Wise, in press) that also attempt to explain other characteristics, such as the observed lack of tangential compression or extension that would be expected with bending.

Calcite twinning analysis provides an independent approach to test the various hypotheses, in particular, as it preserves the early evolution of the belt, prior to regional folding. Results presented here show typical pre-folding, layer-parallel deformation that are sensitive indicators of orogenic evolution, as shown in other studies (e.g., Engelder, 1979a and b; Ferrill and Groshong, 1993a and b; Harris and van der Pluijm, 1998; Kollmeier et al., 2000).

Deformation experiments on limestones have shown that the bulk orientation of calcite twinning in a sample is dependent on the orientation of the remote stress field (Groshong, 1974; Teufel, 1980; Groshong et al., 1984), which can be extracted from natural samples through data inversion techniques (Spang, 1972; Evans and Groshong, 1984). Calcite twinning requires a low critical resolved shear stress of ~10 MPa (Jamison and Spang, 1976; Wenk et al., 1987) and is a strain-hardening process, with further twinning resisted as beds tilt during subsequent deformation. As a consequence, typical deformation conditions recorded are those of the early stress field under horizontal compression, producing layer-parallel shortening fabrics (Jamison and Spang, 1976). A paleostress direction for a sample is derived from a statistical analysis of optimal compression directions for individual twinned calcite grains. This paper focuses on dynamic results from a detailed study along the Pennsylvania salient, which constrains the origin and relative timing of curvature in the belt.

Calcite-twinning Analysis

The analysis of calcite deformation twins (Figure 2) as an indicator of paleostress/strain has yielded reliable results both in experimental (Groshong, 1974; Teufel, 1980; Groshong et al., 1984) and in field studies (Engelder, 1979a and b; Ferril and Groshong, 1993a and b; van der Pluijm et al., 1997; Harris and van der Pluijm, 1998; Kollmeier et al., 2000). Paleostress directions are extracted from a twinned calcite sample by optical determination of the host grain's c-axis and the pole to the e-twin plane within the host (Turner, 1953). This information, along with fixed angular relations between the e-twin pole and grain's c-axis, yields the most favorable orientation of a compression and extension axis for each twinned grain (Figure 3). An aggregate of twinned grains is subsequently analyzed for a dominant (or average) compression direction (Spang, 1972). The analysis can involve routines that invert for the stress tensor (Evans and Groshong, 1994) or traditional contouring analyses using individual axes in an aggregate, both resulting in paleostress directions that reflect the regional stress field. In this study, site directions are analyzed in a geographic as well as in a stratigraphic framework, in order to unravel the syn- and post-twinning deformation history of the host rocks. Since deformational calcite twinning is a strain-hardening process (Teufel, 1980) , it typically records early horizontal compression during layer-parallel shortening (see also, Chinn and Konig, 1973; Engelder, 1979b; van der Pluijm et al., 1997). Similar to other techniques, such as paleomagnetism, this approach can therefore give insight into tectonic rotations, relative timing and direction of compression. If multiple, discrete deformation events occurred, they may be recorded as superimposed populations when the deformations are oriented at a moderate to high angles to one another (Friedman and Stearns, 1971; Teufel, 1980). In these cases, the events can be extracted by discriminating between twins of a dominant compression direction (expected values, or "EVs") and twins of a subordinate compression direction (residual values, or "RVs"), which are determined on the basis of the feasibility of producing the observed twin with a candidate compression direction (Groshong, 1972; Evans and Groshong, 1994).

Oriented samples were collected with a portable, gas-powered diamond coring drill from coarse-grained limestones of the Cambro-Ordovician Beekmantown Group and Siluro-Devonian Keyser, Helderberg, and Tonoloway formations. Beside these units' common occurrence, this stratigraphic sampling strategy offers a test of the Gray and Stamatakos (1997) model that invokes a hidden detachment between these units. Thin sections from oriented samples were optically analyzed on a universal-stage microscope to determine the crystallographic orientations of twin sets and their host calcite grains (Figure 3). To ensure the most accurate possible measurement of the stress field, we confirm that samples are not biased by containing dominantly crystallographically-similarly oriented grains. As well, we only measure twin sets that are straight and continuous within grains, to ensure the most accurate results. Using the dynamic analysis of Turner (1953), we determine the compression axes given the orientation of a grain's c-axis and the twin plane, and derive strain data for each sample using the technique of Groshong (1972). The latter is used to discriminate between expected values (EVs) and residual values (RVs), as suggested by Groshong et al. (1984), in order to clean the data and identify superimposed deformation phases, if any exist. Using the resultant spatial stress distribution we evaluate whether compression was layer-parallel and compare individual site data to geometric models of formation of curved mountain belts.

Results

Calcite twinning analysis of 23 Cambro-Ordovician and 17 Siluro-Devonian sites along the frontal edge of the salient (Figure 1) were quality-evaluated and reduced to provide reliable paleostress directions for 13 Cambro-Ordovician and 15 Siluro-Devonian sites. Reliable paleostress directions were also obtained for 2 sites of Mississippian age in the foreland. Cambro-Ordocivian sites exhibit a dominant population (EVs) of compression directions that are generally orthogonal to regional strike and a residual population (RVs) of subvertical compression directions. Siluro-Devonian sites similarly exhibit a dominant population (EVs) of compression directions orthogonal to regional strike, but also record a small residual population (RVs) of compression directions that are subparallel to strike. We examine in detail only the primary orthogonal signal in both sets of sites as separating the residual populations yields insufficient data for a rigorous analysis of superimposed deformation, but will comment on the likely significance of other populations.

Within the dominant population, most compression axes lie roughly within or near the bedding plane (Figure 4), confirming that twinning records a pre-folding, layer-parallel-shortening fabric. Where tested, directions from oppositely dipping limbs give coherent directions after bedding correction (i.e., positive fold test). Small deviations from parallelism between compression directions with unfolded bedding are expected due to grain-scale rotations during progressive folding, as previously documented in Adirondack calcite twinning (Harris and van der Pluijm, 1998) and Pennsylvania salient paleomagnetic studies (Stamatakos & Hirt, 1994). Whereas the data from sites along the salient show significant scatter, they clearly indicate a fanning pattern of paleostress directions matching changes in regional strike when examined in map view (Figure 5). It is also important to note that this trend is evident in both the Cambro-Ordovician and the Siluro-Devonian data sets, indicating that these units behaved as a structurally coherent package.

We plot paleostress directions as a function of position along the curvature of the salient in order to quantify the observed rotations (Figure 6). Distance along the front is measured from the southwest in a series of linear segments that approximate the along-front distribution of sampling sites (sites that do not fall along the frontal trend of the salient, such as CO-23 and all paleomagnetic sites, are included by projection perpendicular to regional strike). The absence of a difference between Cambro-Ordovician and Siluro-Devonian samples is also clear in this data representation. While there is considerable scatter, the rotational pattern is evident in the raw data and significant at the .001 level with a standard error of the slope of 0.049 and a t-value of 4.3. A moving-average analysis of these data with a conservative interval of n=3 (Figure 7) reduces the inherent scatter in the data and confirms the trend in the raw data set. These moving intervals correspond to 10-40 km segments along the thrust front, yielding a dataset that we compare to representative measurements of regional strike taken every 25 km along the thrust front. Note that regional strike representations show a proportional but lesser scatter than the original calcite data (Figure 6b) and a similar scatter to the moving-averaged calcite data (Figure 7). An excellent match between the slopes of linear best-fits to field and laboratory datasets is observed. By multiplying the best-fit slope of regional strike measurements against the 300 km of sampled frontal distance we obtain a measure of the full curvature of the salient of about 60 degrees. Best-fits to the raw and the moving-averaged data show an equal rotation of paleostress directions of 60-65 degrees along the thrust front, statistically identical to full strike rotation. Analysis of two new sites within the foreland, complementing previously published data (Engelder, 1979a and b), shows no comparable rotation of compression directions in unfolded foreland carbonates, in agreement with regional trends described by Craddock and van der Pluijm (1990) and Craddock et al. (1993).

Discussion

Three populations of compressional directions are observed from calcite twinning analysis in the region: a dominant set of directions roughly orthogonal to regional strike found in both Cambro-Ordovician and Siluro-Devonian sites, a residual set of subvertical directions in Cambro-Ordovician sites, and a residual set of strike-parallel directions restricted to Siluro-Devonian sites.

In the primary population of compressional directions roughly orthogonal to regional strike, no distinction is found between Lower and Middle/Upper Paleozoic units, which contrasts with previous hypotheses requiring a detachment between these sequences (e.g. Gray and Stamatakos, 1997). As shown in Figure 7, the close correspondence of compression directions with regional strike distinct from observations in the foreland shows that primary, oroclinal bending is responsible for the 60° arcuation of the Pennsylvania salient. The scatter in our data is partly inherent in the structure, as shown by the similar scatter in regional strike, but also influenced by grain-scale rotations (Harris and van der Pluijm, 1998) and other superimposed processes.

The small subvertical population evident only in Cambro-Ordovician rocks is attributed to vertical stresses due to overburden during burial or compaction that were not sufficiently large to produce twinning in overlying Siluro-Devonian rocks. The strike-subparallel population occasionally evident in Siluro-Devonian rocks may record localized transpressional stresses. However, the lack of a widespread residual signal indicates the absence of a second regional compression regime that was significantly different in orientation from the first. This contrasts with recent observations from calcite-twinning analysis in the Cantabrian orocline (Kollmeier et al., 2000).

The evidence for the transfer of stresses sufficient for twinning into very weakly deformed continental interior cover rocks (Craddock et al., 1993; van der Pluijm et al., 1997) has important consequences for this study. Because compression directions derived from calcite-twinning analysis predate folding and thrusting in the region, they are therefore the earliest indicator of compression and orogenic evolution (early docking). This allows us to constrain the onset of deformation as post-Middle Carboniferous in age, because rocks of this age exhibit layer-parallel twinning deformation. Evidence for synfolding magnetizations during the early Permian (Stamatakos et al., 1996) brackets the timing of oroclinal deformation between late Carboniferous and early Permian times (i.e., Alleghenian), suggesting late Carboniferous oroclinal rotation. Furthermore, because compression directions from calcite-twinning analysis represent the earliest tectonic signal, all deformation due to subsequent orogenic processes are recorded by the myriad of deformation features seen in the area, such as joint patterns and folding (e.g., Nickelsen, 1979; Gray and Mitra, 1993; Wise, in press). Our work recognizes compression in the earliest time followed by rotations that are not preserved in other deformation features, with the exception of primary paleomagnetic signals (Kent and Opdyke, 1985; Miller and Kent, 1986a,b; Kent, 1988; Stamatakos and Hirt, 1994). While these data (Table 2) display a similar trend of rotation as the calcite-twinning data (Figure 6b), the magnitude of rotation appears to be less than that documented in this study. Nonetheless, these data document a similar change in magnetic direction for this segment of the orocline, commensurate with a change in strike that falls within the calcite data range. It is implicit that other paleomagnetic and structural data with syndeformational acquisition only preserve a partial record of deformation.

We attempt to integrate all available data into a single evolutionary model for the belt (Figure 8). The acquisition of primary magnetization is associated with the deposition of clastic and carbonate rocks in Paleozoic times along the passive margin of Laurentia. Upon collision of Laurentia with Africa, calcite in units as young as mid-Carboniferous become twinned in a dominantly uniform, parallel stress field, a pattern also preserved in foreland carbonates. Strain-hardening locks the initial stress direction as a passive marker in carbonate strata. Next, vertical axis rotations of ~60° displace both the primary magnetic signal and paleostress directions recorded in calcite, providing the bulk of rotations evident in present day. When folding begins prior to the early Permian, regional folds with curved axial surfaces form in their present orientation, following the structural anisotropy imposed by the earlier rotation. Primary curvature explains both the absence of tangential compression or extension (Wise, in press) and limited rotation that is preserved in remagnetized rocks (Gray and Stamatakos, 1997). At the same time, kinematic patterns diverge from their original parallelism to follow the regional pattern of folding. During folding in the early Permian, a secondary (re-) magnetization progresses from the hinterland to the foreland, producing a post-folding magnetization in hinterland folds, a pre-folding magnetization in the, as of yet unfolded, but rotated foreland, and a syn-folding pattern in between (Stamatakos and Gray, 1997). As this fold-related pattern or remagnetization postdates rotation, the past interpretations requiring complicated deformation scenarios are significantly simplified.

Finally, foreland sites from this study and others (Engelder, 1979a and b) suggest convergence to the northwest (present-day coordinates), implying a dextral strike-slip or transpressional regime in the northern segment of the salient and a left-lateral transpressional regime for the southern segment of the Appalachian belt in late Carboniferous times. While residual strike-parallel compression directions in northern salient localities can be attributed to their dextral strike-slip regime, residual directions in the southern part of the salient are more complex. The residual population is more clearly evident in southern localities and shows more scatter, and together with the pattern of along-strike folding that characterizes the region (doubly-plunging anticlines and synclines) supports the concept of a strong transpressional regime for this southern segment of the salient. Comparison of compression directions from within the orocline to those in the foreland yields a close match with the southern limb, implying that this limb was pinned while the northern segment of the salient accommodated most of the rotation in agreement with previously paleomagnetically-determined rotations in the salient (Van der Voo, 1993, p.79). We attribute this pattern to the northerly cratonic presence of Precambrian rocks, the Adirondacks and Reading Prong, which acted as a barrier to northward movement, creating today's Pennsylvania salient. We speculate that lateral variations in wedge thickness as documented by previous workers (Macedo and Marshak, 1999) may also have played a part in the earlier vertical-axis rotations, controlling the development of the structural anisotropy along which folding progressed to produce the curvature in the salient visible today. This influence of basin location and geometry has implications not only for the entire Appalachian chain, showing a series of salients and reentrants, but also to oroclinal belts elsewhere where primary rotations remain to be documented.

Conclusions

Calcite-twinning analysis provides an independent dataset to examine the evolution of the Pennsylvania salient. We have documented a 60° rotation of paleostress directions within the salient, compared to a dominantly uniform stress field preserved in the neighboring foreland and other mid-continental sites. The traditional definition of an orocline is difficult to apply to the salient. Strictly speaking, rotation is of secondary origin, yet the main rotation precedes regional folds, which are curved but unrotated. Instead the belt is better described by a temporally separate evolutionary model of rotation and folding that is able to incorporate new and previously available data. Since convergence directions in the foreland more closely match those of the southern limb of the salient, we suggest that most of the rotation was accommodated in the northern limb as previously suggested by paleomagnetic studies. Furthermore, the north-northwest convergence implies a dextral transpressional regime in this northern segment of the salient and a sinistral regime for the southern segment of the Appalachians. We propose that the rigid cratonic promontory of the Adirondacks and Reading Prong caused rotations, while additionally affected by the lateral variations in sedimentary thickness discussed by others. The Pennsylvania salient, therefore, accommodates the difference in style of Alleghenian deformation between the impinged northern segment and the more mobile southern and central segments of the Appalachians.

Acknowledgements

This project was supported by a grant from the American Chemical Society – Petroleum Research Fund (#37505-AC2), a Geological Society of America Student Research Grant, and the Scott M. Turner Fund of the University of Michigan. We thank Mike Allis for invaluable assistance in the field.

References

Carey, S.W., 1955. The orocline concept in geotectonics. Proc. R. Soc. Tasman., 89, 255-289.

Chinn, A.A., and Konig, R.H., 1973. Stress inferred from calcite twin lamellae in relation to regional structure of northwest Arkansas. Geol. Soc. Am. Bull., 84, 3731-3736.

Craddock, J.P., Jackson, M., van der Pluijm, B.A., and Versical, R.T., 1993. Regional shortening fabrics in eastern North America: far-field stress transmission from the Appalachian-Ouachita orogenic belt. Tectonics, 12, 257-264.

Eldredge, S., Bachtadse, V., and Van der Voo, R., 1985. Paleomagnetism and the orocline hypothesis. Tectonophysics, 119, 153-179.

Engelder, T., 1979a. Mechanisms for strain within the Upper Devonian clastic sequence of the Appalachian Plateau, western New York. Am. J. Sci., 279, 527-542.

Engelder, T., 1979b. The nature of deformation within the outer limits of the central Appalachian foreland fold and thrust belt in New York State. Tectonophysics, 55, 289-310.

Evans, M.A., and Groshong, R.H., 1994. A computer program for the calcite strain-gauge technique. J. Struct. Geol., 16, 277-282.

Fairview, X. No title. Geol. Soc. Am. special paper, in review.

Ferrill, D.A., and Groshong, R.H., 1993. Kinematic model for the curvature of the northern Subalpine Chain, France, J. Struct. Geol., 15, 523-541.

Ferrill, D.A., and Groshong, R.H., 1993. Deformation conditions in the northern Subalpine Chain, France, estimated from deformation modes in coarse-grained limestone. J. Struct. Geol., 15, 995-1006.

Friedman, M., and Stearns, D.W., 1971. Relations between stresses inferred from calcite twin lamellae and macrofractures, Teton Anticline, Montana. Geol. Soc. Am. Bull., 82, 3151-3162.

Geiser, P., and Engelder, T., 1983. The distribution of layer-parallel shortening fabrics in the Appalachian foreland of New York and Pennsylvania: Evidence for two non-coaxial phases of the Alleghenian orogoeny. Geol. Soc. Am. Mem., 158, 161-175.

Gray, M.B., and Mitra, G., 1993. Migration of deformation fronts during progressive deformation: evidence from detailed structural studies in the Pennsylvania Anthracite region, U.S.A. J. Stuct. Geol., 15, 435-449.

Gray, M.B., and Stamatakos, J., 1997. New model for evolution of fold and thrust belt curvature based on integrated structural and paleomagnetic results from the Pennsylvania salient. Geology, 25, 1067-1070.

Groshong, R.H., 1972. Strain calculated from twinning in calcite. Geol. Soc. Am. Bull., 83, 2025-2038.

Groshong, R.H., 1974. Experimental test of least-squares strain gage calculation using twinned calcite. Geol. Soc. Am. Bull., 85, 1855-1864.

Groshong, R.H., Teufel, L.W., and Gasteiger, C., 1984. Precision and accuracy of the calcite strain-gauge technique. Geol. Soc. Am. Bull., 95, 357-363.

Harris, J.H., and van der Pluijm, B.A., 1998. Relative timing of calcite twinning strain and fold-thrust belt development; Hudson Valley fold-thrust belt, New York, U.S.A. J. Struct Geol., 20, 21-31.

Hindle, D., and Burkhard, M., 1999. Strain, displacement and rotation associated with the formation of curvature in fold belts; the example of the Jura arc. J. Struct. Geol., 21, 1089-1101.

Hobbs, W.H., 1914. Mechanics of formation of arcuate mountains. J. Geol., 71-90.

Jamison, W.R., and Spang, J.H., 1976.Use of calcite twin lamellae to infer differential stress. Geol. Soc. Am. Bull., 87, 868-872.

Kent, D.V., and Opdyke, N.D., 1985. Multicomponent magnetization from the Mississipian Mauch Chunk Formation of the central Appalachians and their tectonic implications. J. Geophys. Res., 90, 5371-5383.

Kent, D.V., 1988. Further paleomagnetic evidence for oroclinal rotation in the central folded Appalachians from the Bloomsburg and the Mauch Chunk formations. Tectonics, 7, 749-759.

Kollmeier, J.M., van der Pluijm, B.A., and Van der Voo, R., 2000. Analysis of Variscan dynamics; early bending of the Cantabria-Asturias Arc, northern Spain. Earth Planet. Sci. Lett., 181, 203-216.

Macedo, J., and Marshak, S., 1999. Controls on the geometry of fold-thrust belt salients, Geol. Soc. Am. Bull., 111, 1808-1822.

Marshak, S., 1988. Kinematics of orocline and arc formation in thin-skinned orogens. Tectonics, 7, 73-86.

Miller, J.D., and Kent, D.V., 1986a. Paleomagnetism of the Upper Devonian Catskill Formation from the southern limb of the Pennsylvania salient: Possible evidence of oroclinal rotation. Geophys. Res. Let., 13, 1173-1176.

Miller, J.D., and Kent, D.V., 1986b. Synfolding and prefolding magnetizations in the Upper Devonian Catskill Formation of eastern Pennsylvania: Implications for the tectonic history of Acadia. J. Geophys. Res., 91, 12791-12803.

Nickelsen, R.P., 1979. Sequence of structural stages of the Alleghany orogeny, Bear Valley strip mine, Shamokin, PA. Am. J. Sci., 279, 225-271.

Schwartz, S.Y., and Van der Voo, R., 1983. Paleomagnetic evaluation of the orocline hypothesis in the central and southern Appalachians, Geophys. Res. Lett., 10, 505-508.

Spang, J.H., 1972. Numerical method for dynamic analysis of calcite twin lamellae. Geol. Soc. Am. Bull., 83, 467-472.

Spraggins, S.A., and Dunne, W.M., 2002. Deformation history of the Roanoke recess, Appalachians, USA. J. of Struct. Geol., 24, 411-433.

Stamatakos, J., and Hirt, A.M., 1994. Paleomagnetic considerations of the development of the Pennsylvania salient in the central Appalachians. Tectonophysics, 231, 237-255.

Stamatakos, J., Hirt, A.M., and Lowrie, W., 1996. The age and timing of folding in the central Appalachians from paleomagnetic results. Geol. Soc. Am. Bull., 108, 815-829.

Sun, W., Jackson, M., and Craddock, J.P., 1993. Relationship between remagnetization, magnetic fabric and deformation in Paleozoic carbonates. Tectonophysics, 221, 361-366.

Sussman, A.J., Butler, R.F., Dinares-Turell, J., and Verges, J., 2004. Vertical-axis rotation of a foreland fold and implications for orogenic curvature: an example from the Southern Pyrenees, Spain. Earth and Planet. Sci. Lett., 218, 435-449.

Teufel, L.W., 1980. Strain analysis of experimental superposed deformation using calcite twin lamellae. Tectonophysics, 65, 291-309.

Turner, F.J., 1953. Nature and dynamic interpretation of deformation lamellae in calcite of three marbles. Am. J. Sci., 251, 276-298.

van der Pluijm, B.A., Craddock, J.P., Graham, B.R., and Harris, J.H., 1997. Paleostress in Cratonic North America: Implications for Deformation of Continental Interiors. Science, 277, 794-796.

Van der Voo, R., 1993. Paleomagnetism of the Atlantic, Tethys, and Iapetus oceans. Cambridge University Press, Cambridge, United Kingdom.

Weil, A.B., Van der Voo, R., van der Pluijm, B.A., and Pares, J., 2000. The formation of an orocline by multiphase deformation; a paleomagnetic investigation of the Cantabria Asturias Arc (northern Spain). J. Struct. Geol., 22, 735-756.

Wenk, H.R., Takeshita, T., Bechler, E., Erskine, B.G., and Matthies, S., 1987. Pure shear and simple shear calcite textures. Comparison of experimental, theoretical and natural data. J. Struct. Geol., 9, 731-745.

Wise, D.U., in press. Pennsylvania Salient of the Appalachians: two-azimuth transport model based on new compilations of Piedmont data. Geology.

Younes, A., and Engelder, T., 1999. Fringe cracks: A key data set for the interpretation of progressive Alleghenian deformation of the Appalachian Plateau. Geol. Soc. Am. Bull. 111, 219-239.

Zhou, M., and Jacobi, R.D., 1997. Formation of regional cross-fold joints in the northern Appalachian Plateau. J. Struct. Geol., 19, 817-834.

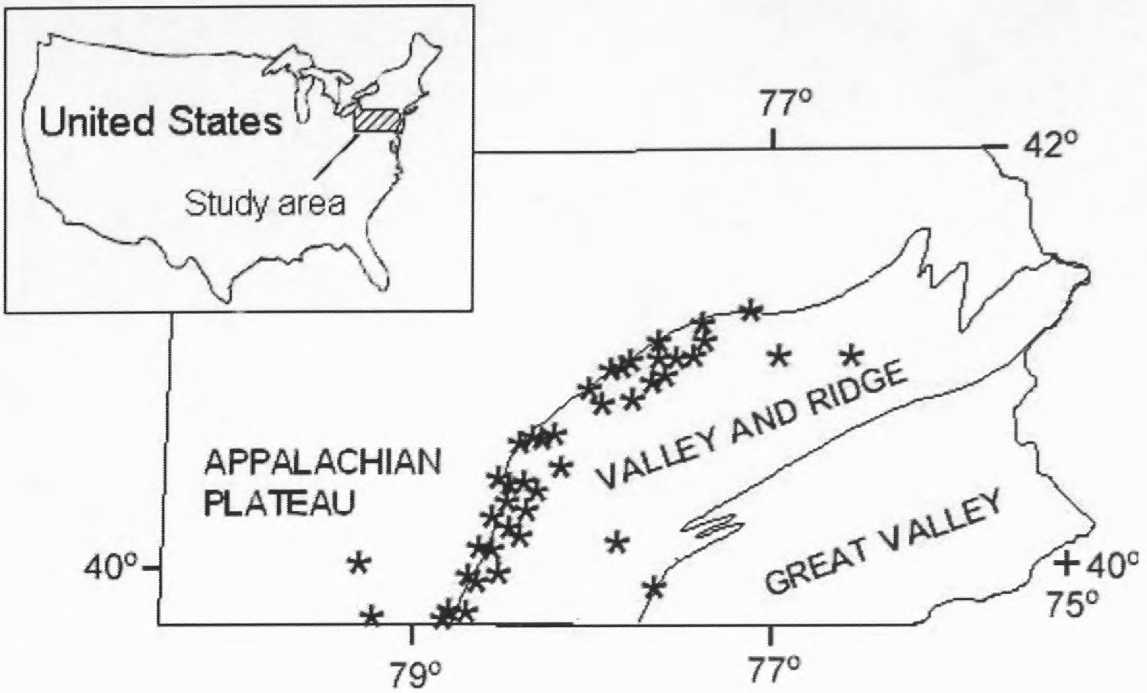

Figure 1. Generalized map of study area, where the Pennsylvania salient follows the outline of the Valley and Ridge province. Stars indictate sampling sites for this study, and province boundaries are schematic.

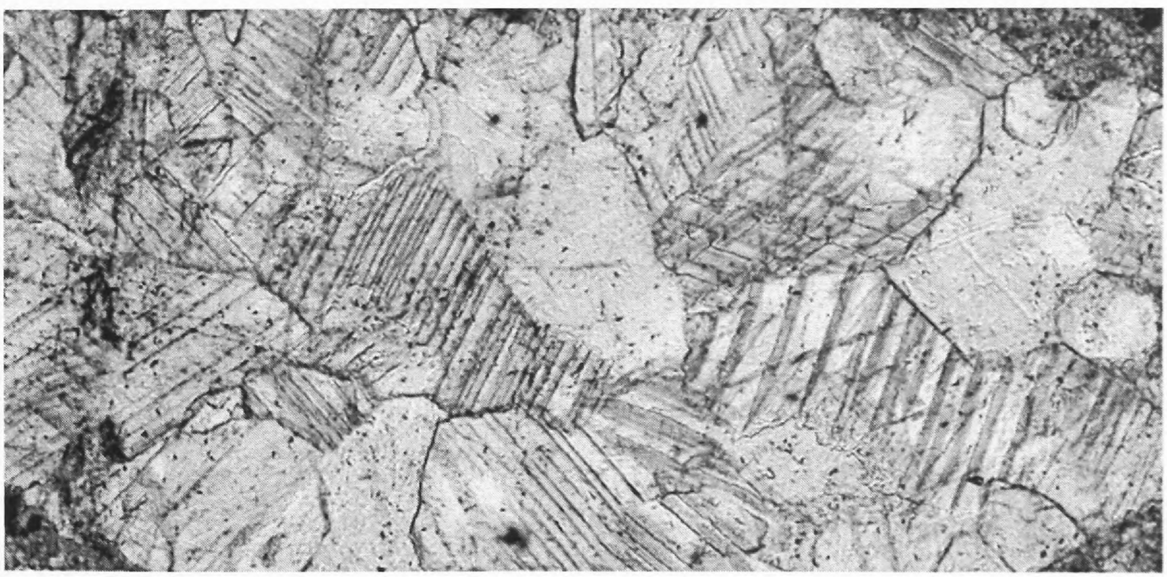

Figure 2. Representative photomicrograph showing twinned calcite grains in plane-polarized light, characterized by single or multiple twin sets and thin twins indicating low-temperature conditions. Width of view is approximately 1 mm.

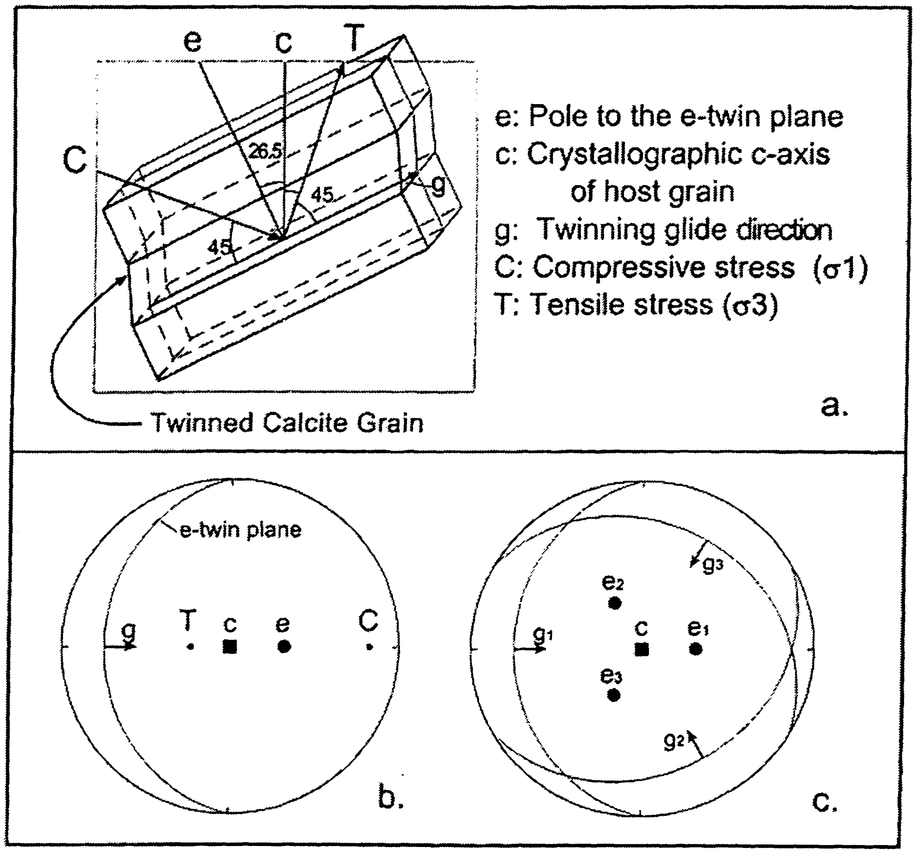

Figure 3. a) A calcite grain with a single e-twin and the compressive (C) and tensile (T) stress axes oriented most favorably to produce twinning (oriented 45° to the e-twin plane). The geometric relation of e-twins to c-axis is fixed. b) The same arrangement as shown in Figure 3a illustrated in a lower-hemisphere equal-area projection, relating the stress orientations to the crystallography. c) All three possible e-twin planes and their poles are represented.

(From Kollmeier et al., 2000)

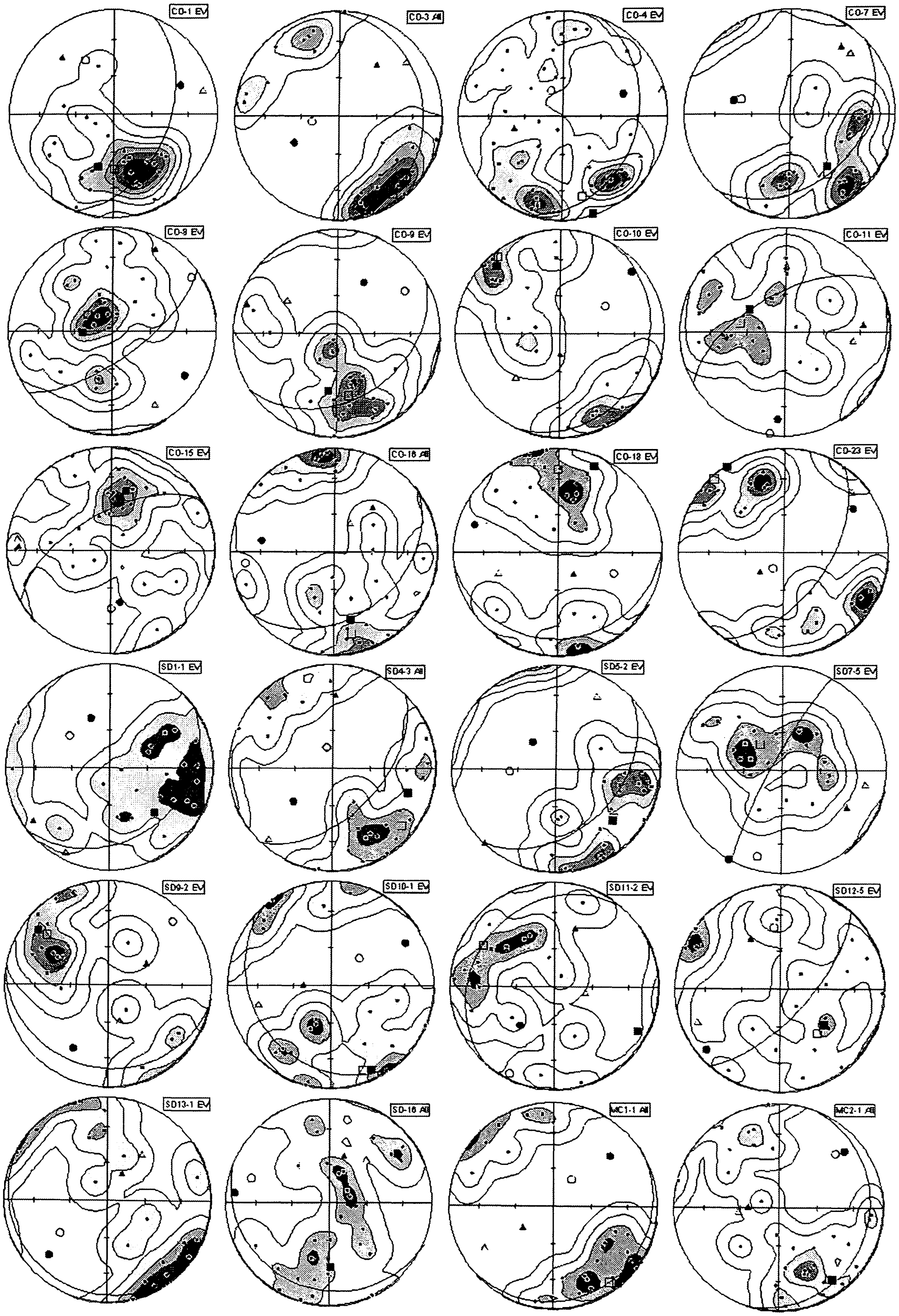
CO-1 EV
CO-3 All
CO-4 EV
CO-7 EV
CO-8 EV
CO-9 EV
CO-10 EV
CO-11 EV
CO-15 EV
CO-16 All
CO-18 EV
CO-23 EV
SD1-1 EV
SD4-3 All
SD5-2 EV
SD7-5 EV
SD9-2 EV
SD10-1 EV
SD11-2 EV
SD12-5 EV
SD13-1 EV
SD-16 All
MC1-1 All
MC2-1 All

Figure 4. Equal-area lower-hemisphere plots of sample results used in this study (unusable and residual results are not shown). Contoured compressive stress axes (small solid circles) are shown as well as the principal stress and strain axes computed using the Strain99 program after the method of Groshong (1972). All data are represented in present-day field coordinates with bedding included. Other symbols: open square – σ_3, open triangle – σ_2, open circle – σ_1; filled square – e_3, filled triangle – e_2, filled circle – e_1.

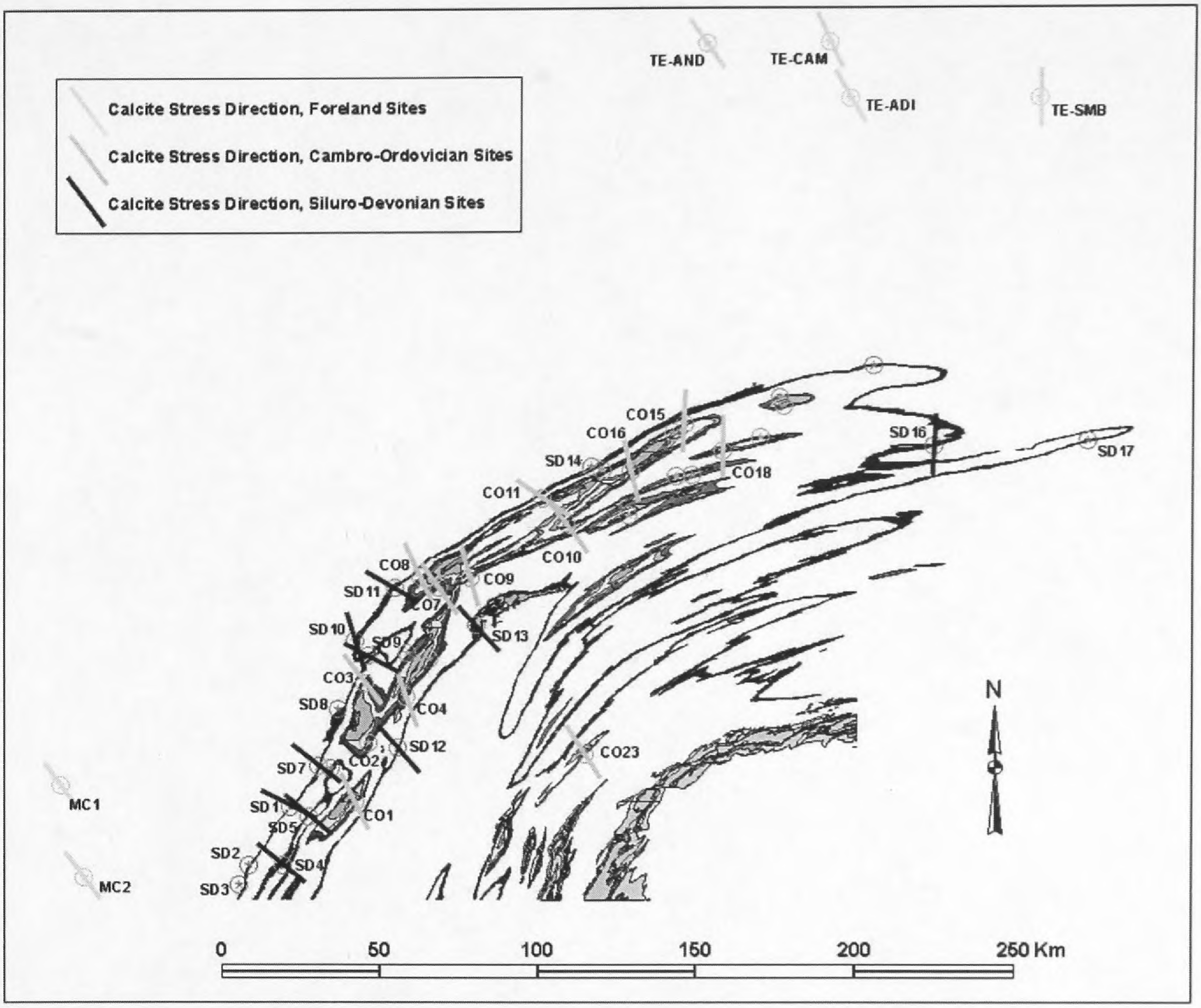

Figure 5. Geographic distribution of tilt-corrected paleostress azimuths (dip-independent) represented by the long direction of bars plotted with respect to geographic north. Bars are shaded according to sample age; dark gray for Cambro-Ordovician, black for Siluro-Devonian, and light gray for all younger, foreland sites. Sites beginning with the "TE" designation are from Engelder (1979a and b). The PA salient is represented by the distribution of limestone units; light grays represent Cambro-Ordovician strata, while blacks represent Siluro-Devonian strata. Site locations are denoted by circled stars – RV sites are labelled but do not have plotted directions, while other unusable sites carry no designation.

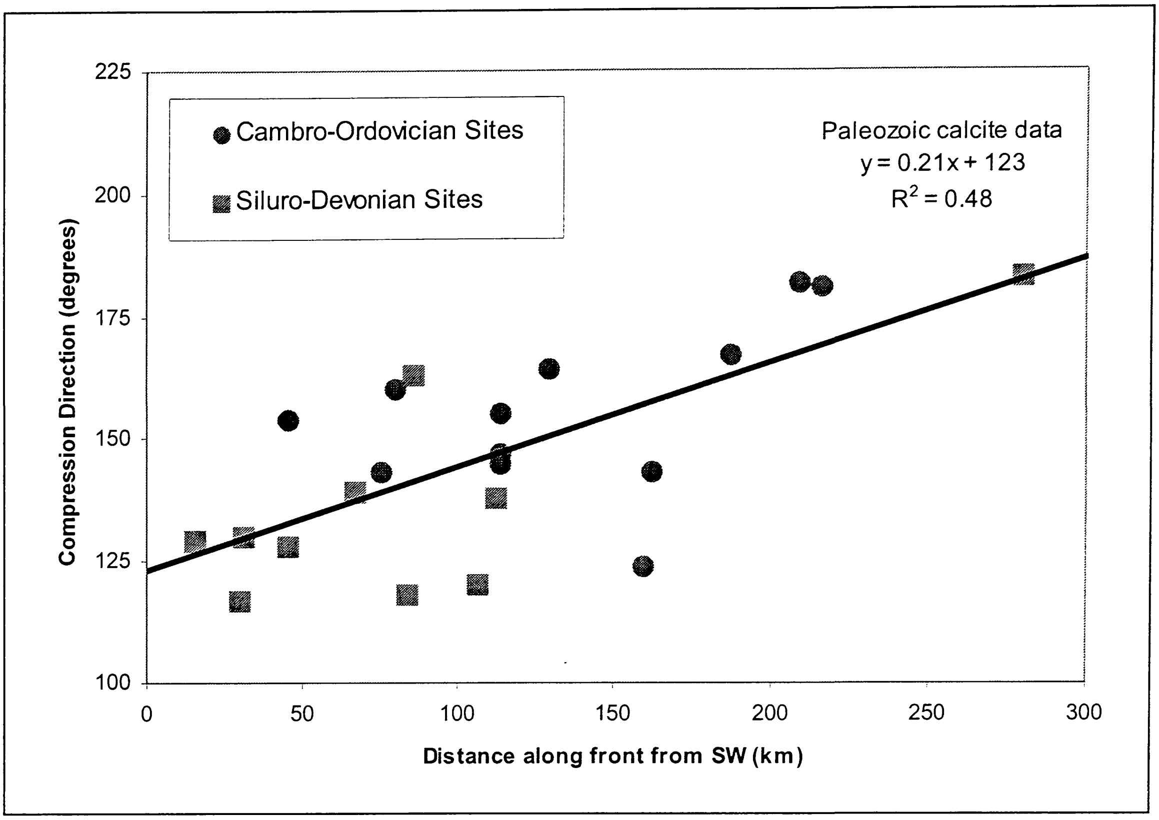

Figure 6a. Calcite stress direction as a function of distance along the thrust front. Cambro-Ordovician sites and Siluro-Devonian sites are distinguished by different symbols, and show no credible difference in rotation. The trendline shown is a simple fit to the combined dataset. Standard error of the slope is 0.049, with a t-value of 4.3, indicating significance of the data set at the .001 level (see text for details).

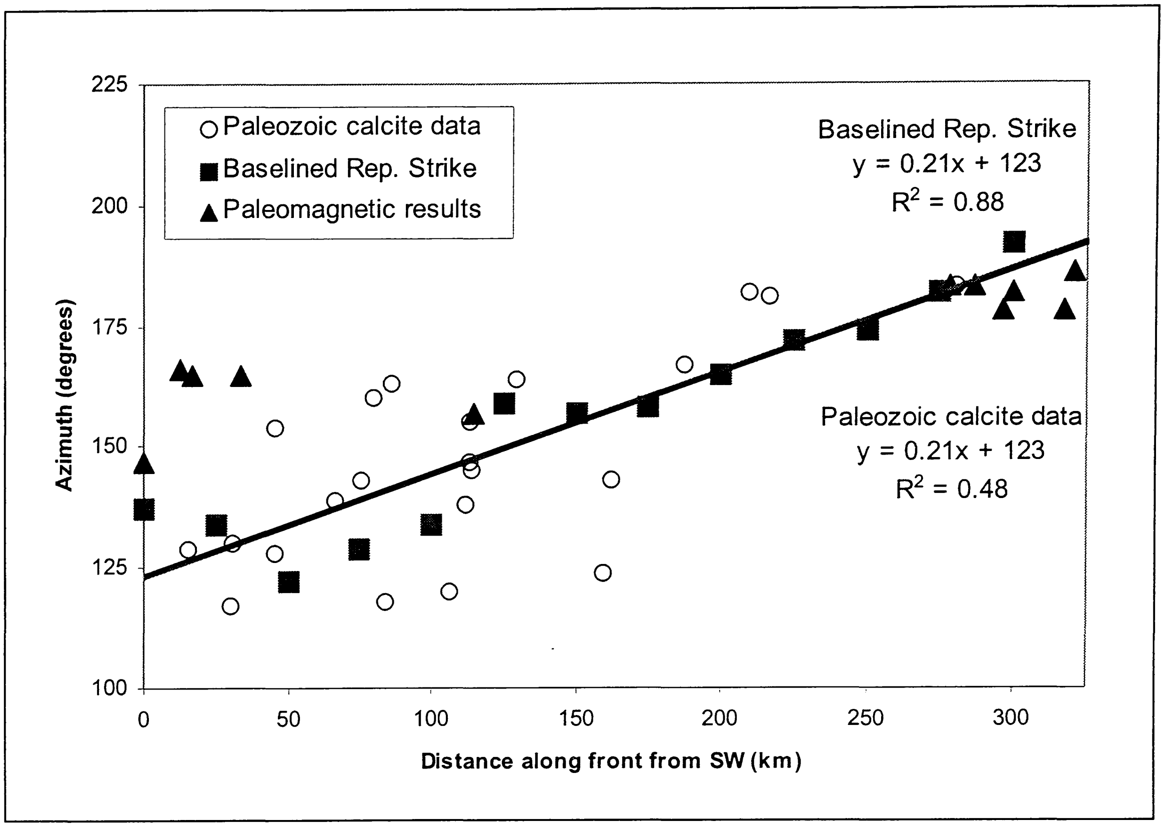

Figure 6b. As above, but including measurements of representative strike and paleomagnetic data for comparison. The trendline through baselined strike is shown and coincides with the trendline of raw data. Paleomagnetic data is summarized in Table 2.

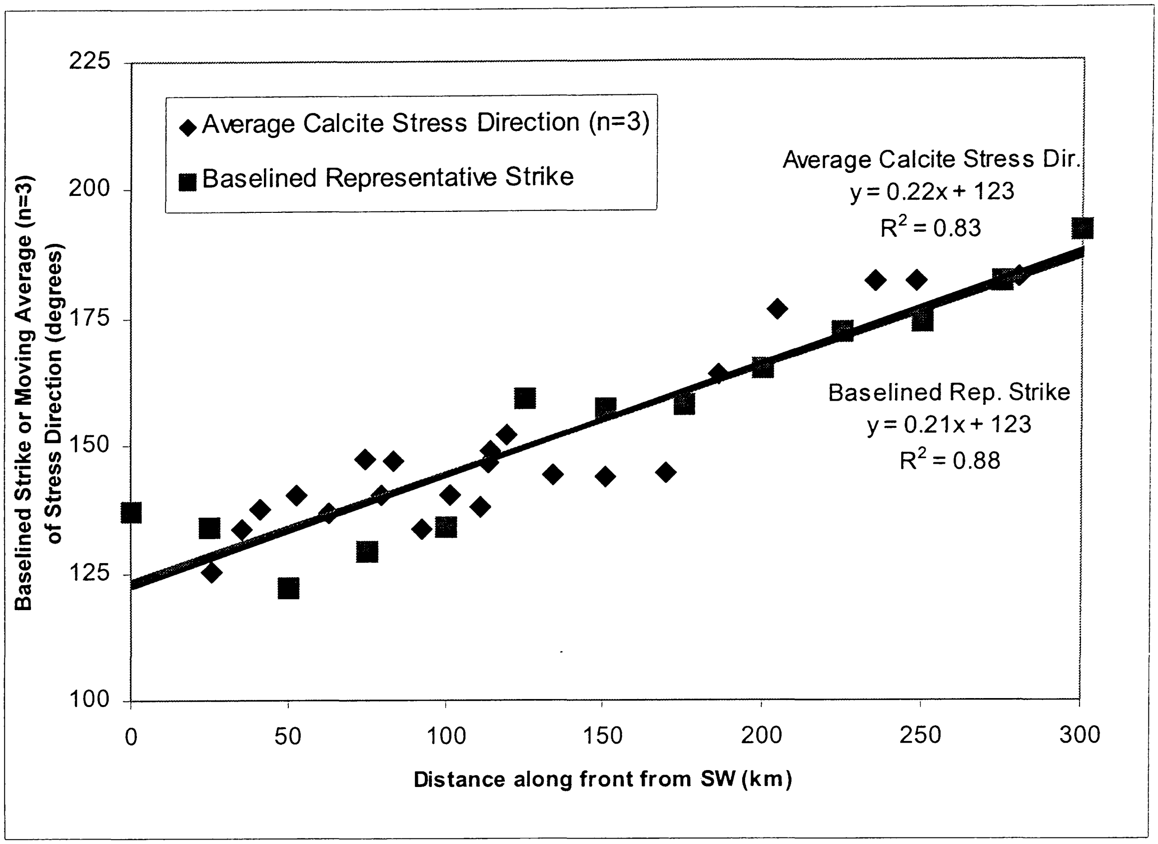

Figure 7. Moving window average analysis of combined calcite paleostress directions, using n=3 (diamonds) as a function of distance along thrust front. Representative strike along the thrust front is plotted schematically with a y-axis shift of 99° for comparison (squares). Best fit lines for both data are shown and fully overlap. The arbitrary value of 99° is used solely because it causes the y-intercepts to coincide and allows for a better visual comparison of the slope.

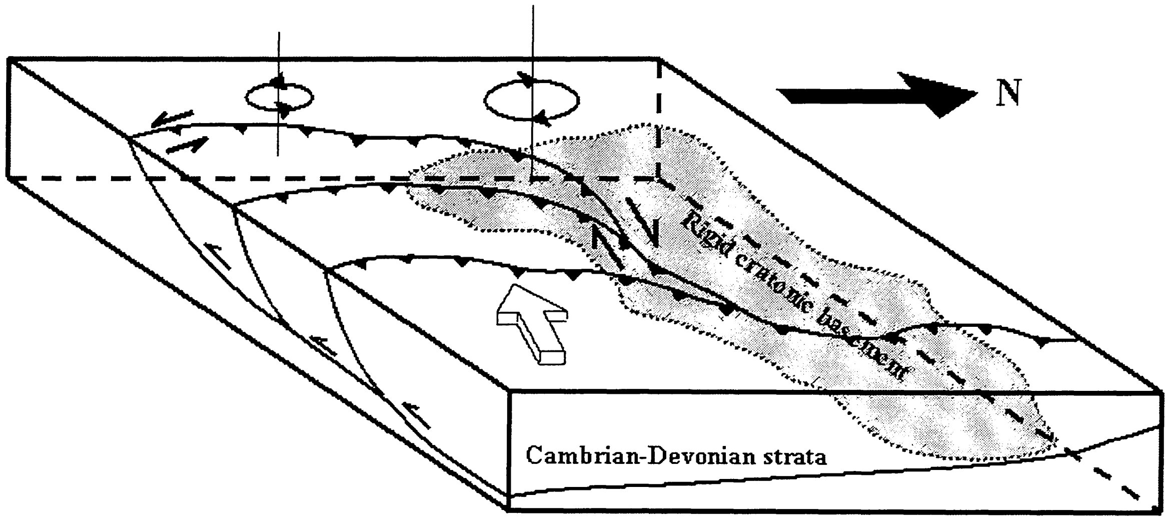

Figure 8. Conceptual model of the evolution of the Pennsylvania salient. After initial collision locks the original paleostress direction through calcite-twinning, vertical axis rotations displace these directions along with primary magnetic signals clockwise in the north and counter-clockwise in the south, with a larger magnitude of rotation in the north. Rotations are induced by lateral variations in stratigraphic thickness as well as impingement upon a rigid cratonic block to the north. Folding and remagnitization occur last, with the present-day salient developing in place along previously defined structural anisotropies.

Site	Lat.	Long.	BC Dist	Strike	Dip	N	St.Err.	% strain	% RV	N RV	Absolute coordinates			Absolute coordinates			Tilt-corrected		Strike	S-S0	D-D0
			km	Sample							e1/elon.	e2/elon.	e3/elon.	sig1	sig2	sig3	sig3	sig3 trd	Regional	Regional	sig3
CO1	40.0023	-78.4200	45.3842	22	46 E	25	1.847	5.1	8	2	(67,32)/4.29	(318,28)/1.37	(196,46)-5.66	332,41	75,13	179,46	154,17	154	41	-7	7
CO3	40.3394	-78.3940	75.2655	-4	20 E	30	0.857	4.7	0	0	(239,49)/4.33	(36,39)/0.67	(136,12)/-5.00	258,69	51,19	145,9	323,1	143	33	-15	-4
CO4	40.3036	-78.2761	79.9156	19	30 E	44	0.258	1.3	14	6	(69,39)/1.25	(256,51)/-0.39	(162,3)/-0.87	335,68	75,4	166,22	160,4	160	39	-9	13
CO7	40.6134	-78.1813	113.6662	44	33 E	22	0.803	4.7	0	0	(284,44)/4.56	(37,21)/0.31	(144,39)/-4.87	287,50	44,20	147,32	325,0	145	51	3	-2
CO8	40.6448	-78.2331	113.5534	54	68 E	24	0.455	2.1	13	3	(122,20)/1.47	(27,12)/0.88	(268,67)/-2.35	56,10	149,20	303,68	155,42	155	49	1	8
CO9	40.6428	-78.0938	129.0225	58	36 E	21	0.333	1.5	5	1	(28,44)/1.51	(288,10)/0.00	(188,44)/-1.51	58,24	303,42	169,39	164,4	164	60	12	17
CO10	40.7985	-77.8234	162.1661	26	17 E	20	0.533	2.2	0	0	(49,11)/2.09	(180,74)/0.11	(317,12)/-2.21	59,48	225,41	321,6	323,22	143	64	16	-4
CO11	40.8668	-77.8864	159.2826	60	60 W	21	0.503	3.5	0	0	(184,18)/3.18	(84,27)/0.61	(303,57)/-3.78	188,3	97,35	281,54	304,4	124	63	15	-23
CO15	41.0780	-77.4870	209.3997	60	60 W	21	0.271	0.9	0	0	(170,48)/0.97	(273,12)/-0.18	(13,40)/-0.78	179,43	277,10	19,45	182,3	182	66	18	35
CO16	40.9428	-77.6391	187.3791	54	36 E	26	0.674	5.6	4	1	(279,30)/3.96	(40,42)/2.46	(166,33)/-6.42	263,15	28,64	168,20	347,13	167	59	11	20
CO18	41.0018	-77.3795	216.3385	84	18 S	20	0.189	0.5	0	0	(288,17)/2.42	(143,69)/0.91	(22,11)/-3.33	111,42	251,40	0,21	1,39	181	73	25	34
CO23	40.1356	-77.7671	113.5534	34	55 E	25	1.127	6.0	0	0	(57,23)/6.49	(231,67)/-1.02	(326,1)/-5.48	212,75	48,14	317,4	327,57	147	46	-2	0
SD1	39.9887	-78.6061	29.7415	54	30 E	23	0.383	2.1	0	0	(339,48)/1.65	(235,12)/0.67	(135,39)/-2.33	309,49	207,9	110,39	117,13	117	40	-8	-30
SD4	39.8196	-78.6253	15.3556	44	52 E	25	0.587	3.4	0	0	(230,49)/3.27	(2,30)/0.34	(108,25)/-3.60	345,73	222,9	130,14	309.38	129	41	-7	-18
SD5	39.9606	-78.5548	30.9155	45	40 E	22	0.657	2.7	0	0	(319,62)/2.87	(224,3)/-0.50	(132,27)/-2.38	267,54	29,21	130,28	310,12	130	40	-8	-17
SD7	40.1069	-78.5259	45.6055	28	82 W	22	0.686	2.3	5	1	(210,1)/3.22	(120,29)/0.09	(302,60)/-3.31	195,15	100,21	320,64	128,16	128	19	-29	-19
SD9	40.4208	-78.3833	83.6574	98	20 S	19	0.571	2.1	5	1	(208,31)1.89	(61,56)/0.42	(307,16)/-2.31	45,14	162,60	309,26	298,34	118	40	-8	-29
SD10	40.4611	-78.4228	85.6198	-40	25 W	21	0.099	0.7	0	0	(60,19)/0.65	(273,68)/0.16	(154,11)/-0.82	46,59	255,29	159,13	163,4	163	35	-13	16
SD11	40.6147	-78.3086	106.5545	40	22 W	20	0.092	0.5	100	20	(221,49)/0.33	(19,40)/0.24	(118,11)/-0.56	207,7	100,65	300,23	300,1	120	50	2	-27
SD12	40.1569	-78.2999	66.5225	42	68 E	20	0.587	4.0	10	2	(230,10)/2.61	(330,43)/1.94	(130,45)/-4.55	354,41	248,17	140,43	319,24	139	21	-27	-8
SD13	40.5088	-78.0737	111.8982	121	10 S	19	0.423	1.7	0	0	(226,24)/1.68	(28,65)/0.04	(134,6)/-1.72	234,44	37,44	136,9	138,6	138	41	-7	-9
SD16	41.0173	-76.7819	280.0040	114	17 S	30	0.726	1.6	17	5	(276,9)/1.77	(17,51)/-0.37	(179,38)/-1.39	287,23	41,45	179,38	183,22	183	79	31	36
																	Average	147	48	0	0
Foreland Population																					
MC1	40.0548	-79.2598	64.9938	55	10 E	25	1.228	4.6	0	0	(48,28)/3.15	(236,61)/2.09	(140,3)/-5.25	34,65	238,24	144,10	324,0	144			
MC2	39.7869	-79.1933	49.1000	18	15 E	30	0.812	4.6	3	1	(49,19)/2.97	(272,66)/2.30	(144,15)/-5.26	46,26	265,59	145,17	143,5	143			
"RV" Population																					
CO2	40.1728	-78.3818	61.2437	12	48 E	44	0.315	2.5	2	1	(256,49)/2.22	(100,39/0.45	(360,12)/-2.67	199,76	90,5	359,14	14,19	194	30	-18	47
SD2	39.8218	-78.7231	7.1506	44	83 W	25	0.612	1.8	4	1	(353,44)/1.92	(252,12)/-0.20	(150,44)/-1.72	336,53	200,28	98,22	17,52	197	35	-17	50
SD3	39.7643	-78.7520	0.0000	-20	3 E	22	0.170	0.8	5	1	(206,69)/0.85	(115,0)/-0.05	(25,21)/-0.80	224,63	114,10	19,25	20,23	200	28	-24	53
SD8	40.2678	-78.4694	64.1509	64	16 W	29	0.227	1.1	0	0	(214,67)/0.78	(113,6)/0.54	(21,23)/-1.32	183,68	277,2	8,22	6,9	186	19	-29	39
SD14	40.9583	-77.7479	177.7241	53	22 N	30	0.591	1.3	17	5	(324,17)/1.51	(88,60)/0.50	(225,23)/-2.01	350,52	151,36	247,9	249,4	249	62	10	102
SD17	41.0300	-76.3491	327.1934	104	42 S	31	0.661	2.2	6	2	(144,35)/2.25	(266,38)/-0.15	(27,33)/-2.10	158,49	269,18	13,36	10,78	190	77	25	43

Table 1. Summary of calcite-twinning analysis results from productive Paleozoic and foreland sites. Summary of sites with an RV-dominant population is also presented.

Site	Lat	Lon	Azimuth	Source
Bloomsburg, PA	41.0	-76.45	186	Stamatakos & Hirt, 1994
Watsontown, PA	41.1	-76.80	183	Stamatakos & Hirt, 1994
Milton, PA	41.0	-76.85	183	Stamatakos & Hirt, 1994
Mt. Union, PA	40.4	-77.85	157	Stamatakos & Hirt, 1994
Cumberland, MD	39.7	-78.70	147	Stamatakos & Hirt, 1994
Hancock, MD	39.7	-78.40	165	Stamatakos & Hirt, 1994
Danville, PA*	40.9	-76.7	178	Stamatakos & Hirt, 1994
Round Top, MD*	39.6	-78.3	166	Stamatakos & Hirt, 1994
D-I*	39.7	-78.1	165	Kent, 1988
J-L, Q-S*	40.9	-76.5	178	Kent, 1988
O, P*	41.0	-76.7	182	Kent, 1988

Table 2. Summary of paleomagnetic data presented in Figure 6b. Latitude and longitude are taken from Stamatakos & Hirt, 1994, Table 1, if available. Sites designated "*" have estimates of latitude and longitude based on the other six sites as well as Stamatakos & Hirt, 1994, Figure 1. Azimuth is taken from Stamatakos & Hirt, 1994, Table 3, modified from stratigraphic declination to lie in the southern quadrants.

Appendix I.

Addendum to Manuals for Calcite Twinning Strain Analysis and Interpretation by John H. Harris, M.Sc. December, 96 and John M. Kollmeier, M.Sc. December, 99.

Philip Ong

Contents

Introduction
I. Sample collection and preparation
II. Optical determination of the c-axis and pole to e-plane of calcite
III. Strain analysis using the CSG22 program
IV. Interpretation and modification of strain analysis
V. Paleostress estimates using calcite twinning data (no additions)

Introduction

This addendum follows up on appendices written by both Harris and Kollmeier, previous U of M calcite-twinning analysis (CTA) students. It provides both clarifying and synthesizing comments building on the previous instructions in an attempt to produce a complete instruction set for CTA, and thus must be used in the context of the previous work.

I. Sample collection and preparation

In this project, only one thin section was made for each site (as opposed to orthogonal sections), with the results showing sufficient accuracy. Care was taken to take into account all rotations of the data from collection in the field to microscope analysis. Namely, this involves: 1) taking the care to polish sample cores as near to orthogonal to the core as possible, so as produce a thin section exactly perpendicular to the core; and 2) measuring any discrepancy between alignment of the core trend direction and the long axis of the slide in order to correct for it later through data rotation.

II. Optical determination of the c-axis and pole to e-plane of calcite

Before any measuring is done, the microscope should be cleaned and checked that all the parts are in alignment, in particular the two polarizers and any of the many graduated mounts of the universal stage. Any misalignment will cause a systematic error in the data collection.

When measuring the c-axis, the correct extinction angle for a calcite grain is almost always the one in which the twin lamellae make an acute (small) angle with the optical vertical. If more than one twin set exists in the grain, then the optical vertical will lie somewhere within the acute angle between the two twin sets at the proper extinction. Developing a consistent method utilizing this fact can save many hours of scope-work.

III. Strain analysis using the calcite strain gauge CSG22 program

The program described in previous work seems to be the same used in this project, except that the version used here is named "Strain99.exe". Unlike previous workers, no rotations were done using this program due to warnings of possible bugs. Instead, all the data was exported and manipulated using one of many stereonet programs, the best of which has been SSWIN because of its interface and versatility.

IV. Interpretation and modification of strain analysis

We adopt the terminology used by Kollmeier, naming both expected values (EVs) and residual values (RVs). Distinction between the two populations greatly helped this project, as it eliminated a lot of "stray" data. The key is to make use of the sample(s) with the highest percent RVs to determine two coexisting populations within the same site, and then categorize the dominant (EV) populations of all other sites within that context. Additionally, bulk analyses on RV populations with a small number of measurement were used, with the knowledge that they carry a larger error, to confirm the presence of multiple populations within the data. While analysis of $n>17$ or optimally $n>20$ provides the most satisfactory trade-off in measurement versus error, analysis of $n<17$ was found to be accurate within 20-25 degrees on a few test cases, and in this context can still be used to distinguish between populations with high angle or nearly orthogonal trends. The presence of these orthogonal populations in this dataset also leads the question of whether two compression events are really necessary to produce orthogonal populations – further study of this phenomenon would be welcome in order to quell any doubts.

Further data cleaning can be done by plotting and contouring the compression axes for each measurement and comparing the results against the bulk stress tensor produced by the Strain99 program. In cases where compression axes showed no pattern, the result was deemed inadequate and dismissed. There are several sites in which the contour patterns seem to produce better results than the output tensor – I speculate that contouring has not been widely incorporated into the procedure before because of the lack of software and computing power to make it an easy task – and in the future, perhaps contouring results can be better incorporated into the analysis.

We interpret a lot of scatter in the data to be due to grain-scale rotations. In principle, data swaths that lie along great circles at high angle to bedding might be extrapolated to result from rotations given a single compression event, which with care might be extracted through manipulation of the data. This might render some sites with steep to overturned bedding more informative, as together with progressive unfolding, they may yield the results of a steady compression direction acting on steadily tilting beds.

V. Paleostress estimates using calcite twinning data

No additions.

Appendix II.

AMS analysis of carbonates of the Pennsylvania salient.

Philip Ong

Introduction

In addition to calcite-twinning analysis, the anisotropy of magnetic susceptibility (AMS) was measured using a Kappabridge machine on a minimum of 6 specimens for every site sampled (results on the following pages). Each specimen is measured in 15 different orientations and fit using a least-squares regression to yield both specimen and site averages. In addition, we measured the bulk susceptibility of representative specimens on an SI2 machine both at room temperature and in liquid nitrogen in order to constrain the magnetic mineralogy.

AMS measurements provide fabrics for 35 sites along the frontal edge of the salient. Most often the minimum susceptibility axis corresponds to the direction yielded by calcite twinning analysis and is taken as the tectonic transport direction, although occasionally intermediate or maximum axes display a closer match. The ratios of low-temperature to room-temperature measurements of bulk magnetic susceptibility show variation around 1 on positive susceptibility measurements, suggesting magnetite of varied grain size as the primary magnetic carrier. Inferred transport directions after bedding correction show a similar pattern of rotation with change in regional strike along the length of the salient.

These results are not readily used because of the difficulty in consistently determining the proper magnetic axis that would correspond to a shortening direction obtained from calcite. Complications include inversion of axes by diamagnetic calcite and complex magnetic mineralogies that vary from sample to sample, even within sites, that render generalizations across samples and sites impossible. All conceived plots of the data – Flinn, P' vs T, P' vs K, T vs K, for example – yielded no clear pattern that might have helped the endeavor. Substantial future work on the mineralogy of these rocks would put the following results in context and allow for a correlation between AMS results and calcite-twinning results. In addition to the results presented here in tabular form, these data are available in electronic format along with a number of different plots of analyses and processing programs.

Sample	T	P'	K	k1	k2	k3	k1/k2	k2/k3	kmax	kint	kmin
A1-1	0.309	1.036	117.93	1.0157	1.0035	0.9808	1.012157449	1.023144372	61,32	177,34	301,39
A1-2	0.136	1.044	156.09	1.0205	1.0018	0.9777	1.0186664	1.024649688	64,29	181,40	310,37
A1-3	0.1	1.038	163.09	1.0179	1.0011	0.981	1.01678154	1.020489297	61,21	167,35	306,48
A1-4	0.11	1.036	152.78	1.0172	1.0012	0.9816	1.015980823	1.0199674	59,19	161,32	303,52
A2-1	-0.055	1.043	169.49	1.0215	0.9991	0.9795	1.022420178	1.020010209	59,59	183,19	281,24
A2-2	0.541	1.052	146.97	1.0199	1.0086	0.9715	1.011203649	1.038188369	40,38	186,47	296,18
B1-1	0.535	1.03	214.22	1.0114	1.0049	0.9837	1.006468305	1.021551286	261,0	1,10	169,80
B1-2	0.616	1.032	193.95	1.0119	1.0061	0.9821	1.005764835	1.02443743	76,6	337,57	170,33
B2-1	0.77	1.023	155.81	1.0079	1.0054	0.9867	1.002486573	1.018952062	343,80	74,0	164,10
B2-2	0.324	1.023	147.76	1.0099	1.0024	0.9877	1.007482043	1.014883062	40,73	255,14	163,9
B3-1	0.781	1.037	248.86	1.0124	1.0086	0.979	1.003767599	1.030234934	88,80	252,9	343,3
B3-2	0.805	1.033	232.05	1.0107	1.0078	0.9816	1.002877555	1.026691117	63,83	261,7	171,2
C1-1	-0.349	1.086	90.45	1.0453	0.9901	0.9645	1.055751944	1.02654225	84,29	246,60	350,8
C1-2	-0.49	1.096	84.87	1.0519	0.985	0.9631	1.067918782	1.022739072	77,28	248,61	345,4
C2-1	-0.901	1.041	68	1.0231	0.9893	0.9876	1.034165572	1.001721345	86,20	221,63	349,18
C3-1	-0.375	1.043	47.23	1.0233	0.9947	0.982	1.028752388	1.01293279	81,14	315,67	175,18
C4-1	-0.004	1.032	61.12	1.0158	0.9999	0.9843	1.01590159	1.015848827	89,3	183,60	357,30
C4-2	-0.379	1.039	70.92	1.0211	0.9952	0.9837	1.02602492	1.011690556	91,11	201,60	355,27
D1-1	0.178	1.044	52.22	1.0203	1.0024	0.9773	1.017857143	1.025683004	64,31	157,6	257,59
D1-2	-0.031	1.03	56.75	1.015	0.9996	0.9854	1.015406162	1.014410392	58,29	152,7	254,60
D2-1	-0.185	1.049	69.9	1.0253	0.9969	0.9778	1.028488314	1.019533647	74,31	176,20	294,52
D2-2	-0.189	1.045	60.75	1.0232	0.9971	0.9797	1.02617591	1.017760539	73,31	173,16	286,55
D3-1	-0.155	1.042	51.75	1.0217	0.9977	0.9805	1.024055327	1.01754207	77,28	175,16	292,57
D3-2	0.314	1.043	44.04	1.0185	1.0042	0.9774	1.014240191	1.027419685	77,30	179,19	297,53
E1-1	0.666	1.037	148.94	1.0131	1.0074	0.9796	1.00565813	1.02837893	225,29	94,50	330,25
E1-2	0.496	1.038	131.83	1.0151	1.0059	0.979	1.009146038	1.027477017	59,2	153,59	327,31
E2-1	0.598	1.034	130.93	1.0128	1.0063	0.9809	1.006459306	1.025894587	176,51	72,11	334,36
E2-2	0.432	1.034	137.66	1.0139	1.0046	0.9815	1.009257416	1.023535405	193,43	81,21	333,39
E3-1	0.716	1.034	141.47	1.0118	1.0073	0.9809	1.004467388	1.026914059	181,48	72,17	328,38
E3-2	0.658	1.039	146.35	1.0141	1.0079	0.978	1.006151404	1.030572597	195,40	79,28	324,37
F1-1	0.176	1.03	43.56	1.0136	1.0016	0.9847	1.011980831	1.017162588	53,15	292,62	150,23
F2-1	-0.06	1.03	53.16	1.0153	0.9993	0.9854	1.016011208	1.014105947	58,25	304,41	170,39
F2-2	-0.062	1.029	53.42	1.0145	0.9993	0.9862	1.015210647	1.01328331	62,14	312,55	160,32
F3-1	0.909	1.027	75.21	1.0082	1.0071	0.9847	1.001092245	1.022748045	76,4	343,42	171,48
F4-1	-0.126	1.029	67.89	1.0149	0.9987	0.9864	1.016221087	1.012469586	61,4	323,64	153,25
F4-2	0.365	1.025	66.86	1.0107	1.0029	0.9864	1.007777445	1.016727494	59,17	303,55	159,29
G1-1	-0.674	1.019	25.03	1.0105	0.9961	0.9933	1.01445638	1.002818887	239,11	139,41	341,47
G1-2	0.066	1.012	35.54	1.006	1.0003	0.9937	1.005698291	1.006641844	222,10	328,57	126,32
G2-1	0.566	1.03	49.61	1.0112	1.0052	0.9836	1.005968961	1.021960146	42,8	294,65	135,23
G2-2	-0.54	1.032	48.71	1.0176	0.9946	0.9878	1.023124874	1.006883985	234,7	355,77	143,11
G3-1	0.197	1.037	49.25	1.0167	1.0022	0.9811	1.01446817	1.021506472	59,20	299,55	160,28
G3-2	0.593	1.051	34.59	1.0189	1.0091	0.972	1.009711624	1.038168724	289,49	50,25	156,31

Sample	T	P'	K	k1	k2	k3	k1/k2	k2/k3	kmax	kint	kmin
H1-1	0.044	1.069	141.62	1.0328	1.0006	0.9666	1.032180692	1.03517484	246,11	128,67	340,20
H1-2	-0.337	1.053	189.17	1.0283	0.9941	0.9775	1.034402978	1.016982097	256,4	160,54	349,36
H1-3	-0.201	1.049	140.65	1.0257	0.9966	0.9777	1.029199278	1.019331083	77,4	170,40	342,50
H2-1	0.284	1.076	137.78	1.033	1.0064	0.9606	1.026430843	1.047678534	83,7	183,54	348,35
H3-1	0.132	1.077	87.28	1.0356	1.0028	0.9616	1.032708416	1.042845258	249,7	148,57	344,32
H4-1	0.497	1.059	144.32	1.023	1.0089	0.9681	1.013975617	1.042144407	266,20	162,35	20,48
I1-1	0.399	1.018	220.11	1.0077	1.0023	0.9899	1.005387609	1.012526518	283,29	42,41	170,36
I2-1	0.162	1.016	208.99	1.0073	1.0008	0.9919	1.006494804	1.008972679	283,38	45,35	162,34
I3-1	0.536	1.012	211.39	1.0047	1.002	0.9933	1.002694611	1.008758683	281,19	31,45	175,39
I3-2	-0.659	1.029	169.85	1.0165	0.994	0.9895	1.022635815	1.004547751	1,49	118,22	223,33
I4-1	0.222	1.022	142.96	1.0099	1.0016	0.9885	1.008286741	1.013252403	4,68	274,0	184,22
I4-2	0.136	1.021	141.31	1.0097	1.0009	0.9894	1.008792087	1.011623206	349,68	94,6	187,21
J1-1	0.357	1.034	137.25	1.0144	1.0038	0.9818	1.010559872	1.022407822	300,47	67,30	175,28
J2-1	0.571	1.036	69.7	1.0136	1.0063	0.9801	1.007254298	1.026731966	91,27	262,63	359,4
J2-2	0.372	1.042	122.12	1.0177	1.0049	0.9774	1.012737586	1.028135871	284,44	105,46	15,0
J3-1	-0.52	1.044	131.75	1.0242	0.9928	0.983	1.03162772	1.009969481	285,41	34,20	143,42
J4-1	-0.258	1.036	62.02	1.0193	0.9968	0.9838	1.022572231	1.013214068	255,9	130,74	347,13
J4-2	-0.081	1.035	66.12	1.0179	0.999	0.9832	1.018918919	1.016069976	74,8	267,82	165,2
K1-1	-0.843	1.056	171.12	1.0317	0.986	0.9822	1.046348884	1.003868866	327,53	125,35	222,11
K2-1	-0.043	1.055	125.67	1.0271	0.999	0.9739	1.028128128	1.025772667	304,64	67,14	162,21
K3-1	-0.138	1.049	128.04	1.0248	0.9976	0.9775	1.027265437	1.02056266	336,66	243,1	153,24
K3-2	-0.127	1.052	127.66	1.0263	0.9977	0.976	1.028665932	1.022233607	342,59	247,3	155,31
K4-1	-0.855	1.062	134.49	1.0351	0.9844	0.9805	1.051503454	1.003977562	336,61	228,10	133,27
K4-2	-0.698	1.059	160.27	1.0333	0.9873	0.9794	1.046591715	1.008066163	338,57	228,12	131,30
L1-1	-0.549	1.051	17.54	1.028	0.9912	0.9808	1.037126715	1.010603589	75,7	168,22	328,67
L1-2	-0.606	1.055	20.91	1.0304	0.9897	0.9799	1.041123573	1.010001021	82,10	278,80	172,3
L2-1	-0.233	1.09	25.13	1.0465	0.9927	0.9607	1.054195628	1.033309045	72,10	172,44	332,44
L2-2	-0.672	1.066	26.05	1.0366	0.9865	0.977	1.050785606	1.009723644	74,5	168,36	337,53
L2-3	-0.708	1.066	42.19	1.0369	0.9858	0.9773	1.051836072	1.008697432	76,4	188,80	345,9
L3-1	0.004	1.061	29.34	1.0296	0.9998	0.9706	1.029805961	1.030084484	70,8	170,50	334,38
M1-1	-0.082	1.087	354.97	1.043	0.9972	0.9599	1.0459286	1.038858214	86,21	259,69	356,2
M1-2	0.158	1.079	297.59	1.0359	1.0035	0.9606	1.032286996	1.044659588	91,18	245,70	358,8
M2-1	-0.299	1.068	237.4	1.0362	0.9931	0.9707	1.043399456	1.023076131	88,4	312,84	178,4
M2-2	-0.068	1.07	291.46	1.035	0.9981	0.9669	1.036970243	1.032268073	86,3	338,79	176,10
M3-1	0.048	1.077	280.2	1.0369	1.0007	0.9624	1.036174678	1.039796342	77,10	273,80	167,3
M3-2	-0.06	1.081	267.52	1.0401	0.9979	0.9619	1.042288806	1.037425928	69,17	245,73	338,1
N'4-1	-0.848	1.055	7.59	1.0309	0.9863	0.9827	1.045219507	1.003663376	48,23	140,7	245,66
N'4-2	-0.557	1.042	11.43	1.0232	0.9927	0.9842	1.030724287	1.008636456	43,26	139,11	250,61
N'5-1	-0.517	1.011	36	1.0062	0.9982	0.9956	1.008014426	1.002611491	249,9	345,34	146,54
N'5-2	-0.381	1.024	27.96	1.0129	0.9971	0.99	1.015845953	1.007171717	232,21	323,4	64,68
N'6-1	0.589	3.259	-0.36	-0.4621	-1.1239	-1.414	0.411157576	0.794837341	40,17	141,30	284,54
N'7-1	-0.594	1.025	20.19	1.0138	0.9954	0.9908	1.018485031	1.004642713	280,28	22,22	145,53
O1-1	0.649	1.032	80.65	1.0117	1.0064	0.9819	1.005266296	1.024951624	96,29	211,36	339,40
O1-2	0.563	1.036	81.12	1.0136	1.0062	0.9801	1.007354403	1.026629936	116,36	233,31	351,38
O2-1	-0.454	1.032	128.51	1.0175	0.9953	0.9872	1.022304833	1.008205024	266,1	175,37	357,53
O2-2	-0.246	1.04	130.84	1.0209	0.9967	0.9824	1.024280124	1.014556189	249,19	139,46	354,38
O3-1	0.266	1.035	88.49	1.0156	1.0029	0.9815	1.012663276	1.021803362	137,41	252,26	5,38
O3-2	0.594	1.027	98.37	1.01	1.0049	0.9851	1.005075132	1.020099482	155,47	263,16	6,38

Sample	T	P'	K	k1	k2	k3	k1/k2	k2/k3	kmax	kint	kmin
P1-1	-0.757	1.05	250.02	1.0282	0.9886	0.9832	1.040056646	1.00549227	100,10	328,75	192,11
P1-2	-0.942	1.053	245.68	1.03	0.9857	0.9844	1.04494268	1.001320601	99,5	1,62	192,28
P2-1	-0.795	1.06	258.81	1.0338	0.9858	0.9804	1.048691418	1.005507956	278,12	18,38	173,50
P2-2	-0.62	1.059	247.86	1.0328	0.9887	0.9786	1.044604025	1.010320867	281,9	14,18	166,69
P3-1	-0.616	1.06	253.56	1.0334	0.9885	0.9781	1.045422357	1.01063286	110,6	16,32	210,57
P3-2	-0.817	1.056	242.03	1.0318	0.9863	0.9819	1.046132009	1.004481108	107,7	356,71	200,18
Q1-1	0.444	1.018	378.79	1.0072	1.0025	0.9903	1.004688279	1.012319499	131,67	286,21	20,9
Q2-1	-0.16	1.012	385.75	1.0062	0.9994	0.9944	1.006804082	1.005028158	106,12	359,53	205,35
Q3-1	-0.091	1.02	346.42	1.0101	0.9994	0.9905	1.010706424	1.008985361	73,61	296,22	198,18
Q4-1	0.937	1.013	246.3	1.0039	1.0036	0.9925	1.000298924	1.011183879	342,83	95,3	185,7
Q4-2	0.834	1.014	222.41	1.0047	1.0036	0.9917	1.001096054	1.011999597	293,43	84,43	189,15
Q4-3	0.59	1.016	194.39	1.0062	1.003	0.9908	1.003190429	1.012313282	307,29	95,56	209,15
R1-1	-0.2	1.048	34.33	1.0249	0.9967	0.9783	1.028293368	1.018808137	101,1	192,38	10,52
R1-2	-0.192	1.047	41.7	1.0245	0.9969	0.9786	1.027685826	1.018700184	96,6	190,36	357,54
R2-1	-0.068	1.04	40.05	1.0201	0.999	0.981	1.021121121	1.018348624	96,14	213,61	359,25
R2-2	-0.466	1.034	38.86	1.0187	0.9949	0.9864	1.023922002	1.008617194	91,11	189,36	347,52
R3-1	-0.398	1.048	43.08	1.0259	0.9938	0.9803	1.032300262	1.013771295	278,1	186,50	8,40
R3-2	-0.121	1.045	45.02	1.0229	0.9981	0.979	1.02484721	1.019509704	283,1	193,30	16,60
S1-1	0.286	1.035	22.3	1.0152	1.0031	0.9817	1.012062606	1.02179892	358,6	88,3	203,84
S1-2	-0.132	1.042	19.19	1.0216	0.998	0.9804	1.023647295	1.017951856	22,16	289,11	168,70
S2-1	0.627	1.048	20	1.0175	1.0091	0.9734	1.008324249	1.03667557	269,3	0,25	171,65
S2-2	0.358	1.046	17.68	1.0194	1.0051	0.9754	1.01422744	1.030449047	358,9	90,8	222,78
S3-1	0.38	1.031	10.89	1.0132	1.0038	0.983	1.009364415	1.021159715	53,13	313,37	159,50
S3-2	0.388	1.035	14.23	1.0148	1.0043	0.9809	1.010455043	1.023855643	24,26	276,32	145,47
T1-1	-0.034	1.035	199.84	1.0173	0.9995	0.9832	1.017808904	1.016578519	270,4	78,86	180,1
T1-2	-0.023	1.033	191.93	1.0163	0.9997	0.984	1.016604981	1.015955285	272,6	49,82	182,5
T2-1	-0.103	1.035	234.65	1.0178	0.9987	0.9835	1.019124862	1.015455008	256,0	350,84	166,6
T2-2	-0.04	1.028	222.41	1.0139	0.9996	0.9865	1.014305722	1.01327927	260,7	31,80	169,8
T3-1	0.265	1.033	230.72	1.0147	1.0028	0.9825	1.011866773	1.020661578	262,5	57,84	171,2
T3-2	0.085	1.034	227.56	1.0164	1.0009	0.9828	1.015486063	1.018416768	266,8	61,81	176,4
U1-1	0.059	1.048	30.92	1.023	1.0007	0.9763	1.022284401	1.024992318	261,16	141,60	359,24
U1-2	0.148	1.045	44.39	1.0211	1.002	0.9769	1.019061876	1.02569352	262,14	143,64	358,22
U1-3	0.048	1.048	32	1.0234	1.0006	0.9761	1.022786328	1.025099887	267,13	154,59	4,28
U2-1	-0.097	1.078	32.53	1.0389	0.9971	0.964	1.041921573	1.0343361	257,2	163,61	348,29
U3-1	0.044	1.044	26.59	1.0212	1.0005	0.9783	1.020689655	1.022692426	82,4	208,84	351,5
U3-2	-0.223	1.047	37.99	1.0247	0.9964	0.9789	1.028402248	1.017877209	85,5	192,73	353,16
V1-1	-0.461	1.139	39.01	1.0736	0.9795	0.9469	1.096069423	1.034428134	240,15	4,64	144,21
V1-2	-0.625	1.133	41.77	1.0723	0.9745	0.9532	1.100359159	1.022345783	241,18	9,62	143,20
V2-1	-0.381	1.14	65.62	1.0732	0.9825	0.9443	1.092315522	1.040453246	237,10	335,41	136,47
V2-2	-0.445	1.149	68.11	1.0784	0.9787	0.9429	1.101869827	1.037967971	238,12	342,46	137,41
V3-1	-0.494	1.129	59.35	1.0691	0.9797	0.9511	1.091252424	1.030070445	242,17	355,53	141,32
V4-1	-0.55	1.15	32.41	1.0804	0.9742	0.9454	1.109012523	1.030463296	239,16	350,51	138,34
MC1-2A	-0.245	1.009	76.18	1.0048	0.9993	0.996	1.005503853	1.003313253	29,33	144,33	267,40
MC1-3A	-0.332	1.012	60.47	1.0066	0.9987	0.9947	1.007910283	1.004021313	52,1	318,72	142,18
MC1-4A	-0.066	1.017	57.38	1.0085	0.9996	0.9919	1.008903561	1.007762879	227,22	88,62	324,17
MC1-4B	-0.365	1.015	59.44	1.0079	0.9983	0.9938	1.009616348	1.004528074	234,2	103,60	332,20
MC1-5A	-0.235	1.013	61.28	1.0069	0.999	0.9941	1.007907908	1.004929082	57,7	204,82	326,4
MC1-6A	-0.261	1.015	54.17	1.0082	0.9887	0.9931	1.019722868	0.995569429	59,8	236,82	329,0
MC1-7A	0.68	1.101	365.6	1.0343	1.0197	0.946	1.014317937	1.077906977	239,10	146,14	4,73

Sample	T	P'	K	k1	k2	k3	k1/k2	k2/k3	kmax	kint	kmin
MC2-1A	-1	1.02	5.54	1.0115	0.9943	0.9943	1.017298602	1	21,43	133,22	242,39
MC2-1B	0.635	1.059	7.14	0.9889	1.0156	0.9675	0.973710122	1.049715762	35,27	155,45	286,33
MC2-2A	-1	1.042	5.28	0.9889	1.024	0.988	0.965722656	1.036437247	203,0	113,88	293,2
MC2-2B	0.664	1.059	6.16	1.0052	1.0206	0.9678	0.984910837	1.054556727	23,0	113,66	293,24
MC2-3A	0.666	1.072	6.23	1.0204	1.0127	0.9669	1.007603436	1.047367877	8,49	212,38	112,12
MC2-5A	-0.277	1.054	6.37	0.955	1.0249	0.9801	0.931798224	1.045709621	220,12	328,55	122,32
MC2-6A	-1	1.017	6.41	0.995	1.0025	1.0025	0.992518703	1	77,13	307,70	171,15
SD1-1A	0.003	1.01	16.42	0.9971	1.0029	1	0.994216771	1.0029	207,4	298,15	104,74
SD1-2A	0.445	1.021	19.7	0.9903	1.0073	1.0024	0.983123201	1.004888268	232,10	139,15	356,72
SD1-3A	0.66	1.012	29.79	1.0016	1.012	0.9952	0.98972332	1.016881029	49,17	317,26	213,72
SD1-4A	0.146	1.012	28.89	0.9989	0.9989	1.0022	1	0.996707244	199,5	100,63	292,26
SD1-5A	0.166	1.007	34.13	0.9972	1	1.0028	0.9972	0.997207818	150,51	59,1	328,39
SD1-5B	0.003	1.01	29.9	1.005	1	0.995	1.005	1.005025126	82,4	180,63	350,27
SD1-6A	0.079	1.025	16.61	0.9914	1.0115	0.9872	0.980128522	1.024615073	239,8	331,17	126,71
SD2-1A	-0.328	1.031	17.67	1.0164	0.9967	0.9869	1.019765225	1.009930084	211,37	4,50	111,13
SD2-1B	-0.076	1.021	20.55	1.0105	0.9994	0.9901	1.011106664	1.009392991	209,35	336,41	95,30
SD2-2A	0.034	1.022	14.98	1.0106	1.0002	0.9892	1.01039792	1.011120097	232,24	12,59	134,18
SD2-3A	-0.016	1.017	21.02	0.9992	0.9924	1.0083	1.006852076	0.984230884	206,41	59,44	312,17
SD2-3B	-0.405	1.037	22.84	1.0203	0.9951	0.9846	1.025324088	1.010664229	261,86	26,2	116,3
SD2-4A	0.348	1.031	20.95	1.0133	1.0034	0.9833	1.009866454	1.020441371	7,27	241,49	112,28
SD3-1A	0.771	1.134	27.01	0.9383	1.0406	1.0212	0.901691332	1.018997258	354,5	263,6	122,82
SD3-1B	0.57	1.121	18.78	0.9391	1.0431	1.0177	0.900297191	1.024958239	341,4	71,2	192,85
SD3-2A	0.555	1.125	28.81	0.9377	1.0419	1.0204	0.899990402	1.021070169	167,3	257,4	34,85
SD3-3A	0.166	1.03	57.61	1.014	1.0016	0.9845	1.012380192	1.017369223	340,4	250,3	127,85
SD3-4A	-0.361	1.052	384.86	0.9957	1.0037	1.0006	0.992029491	1.003098141	2,18	141,67	268,15
SD3-4B	-0.028	1.046	335.49	0.9938	1.0084	0.9776	0.985521618	1.031505728	359,19	111,48	255,36
SD4-1A	0.47	1.076	30.5	1.0297	1.0106	0.9597	1.018899664	1.053037408	57,18	170,50	314,34
SD4-1B	0.216	1.043	36.05	0.9978	0.9859	1.0163	1.01207019	0.970087573	61,13	175,61	325,26
SD4-2A	0.677	1.04	50.22	1.0003	0.9937	1.006	1.006641844	0.98777336	224,10	117,58	320,30
SD4-3A	0.906	1.046	28.06	0.9825	1.0096	1.0079	0.973157686	1.001686675	86,33	181,8	283,56
SD4-4A	-0.044	1.04	49.31	0.9936	0.9916	1.0148	1.002016942	0.977138352	54,12	167,62	318,25
SD4-5A	0.232	1.048	36.47	1.0215	1.0034	0.9751	1.018038669	1.029022664	50,5	151,65	318,25
SD5-1A	-0.379	1.016	51.15	1.0025	0.9997	0.9978	1.00280084	1.001904189	260,5	155,71	351,18
SD5-2A	-0.634	1.085	116	0.9943	1.0127	0.993	0.981830749	1.019838872	124,43	12,22	263,39
SD5-3A	-0.187	1.082	142.65	1.042	0.9946	0.9634	1.04765735	1.032385302	119,43	18,11	277,45
SD5-3B	-0.258	1.095	151.49	1.0493	0.9916	0.9591	1.058188786	1.033885935	122,43	25,7	289,46
SD5-4A	-0.144	1.083	149.98	0.9844	1.0143	1.0013	0.970521542	1.012983122	125,38	19,20	268,45
SD5-5A	-0.622	1.079	132.47	1.0438	0.9847	0.9714	1.06001828	1.013691579	119,36	227,24	344,45
SD6-1A	0.274	1.093	285.97	0.9924	0.9987	1.009	0.993691799	0.989791873	289,19	73,67	194,12
SD6-1B	0.357	1.09	317.96	0.9953	1.0027	1.002	0.992619926	1.000698603	284,23	79,65	190,10
SD6-2A	0.583	1.084	347.95	1.0307	1.0144	0.9549	1.016068612	1.06231019	290,23	78,63	194,13
SD6-3A	0.608	1.088	319.77	1.0316	1.0157	0.9528	1.015654229	1.066015953	287,12	108,78	17,0
SD6-4A	0.299	1.091	32.74	0.9568	1.031	1.0121	0.928031038	1.018674044	99,10	8,6	245,78
SD6-4B	0.187	1.058	33.74	0.9713	1.0235	1.0052	0.948998534	1.018205332	96,5	186,4	314,84
SD6-5A	0.476	1.063	368.66	1.0246	1.009	0.9663	1.015460852	1.044189175	294,8	39,64	200,24

Sample	T	P'	K	k1	k2	k3	k1/k2	k2/k3	kmax	kint	kmin
SD7-1A	-0.475	1.033	85.19	1.0175	0.9868	0.9867	1.031110661	1.000101348	291,86	131,4	41,1
SD7-1B	-0.611	1.033	118.82	1.0186	0.9937	0.9877	1.025057865	1.006074719	288,73	82,62	262,28
SD7-2A	-0.162	1.038	101.41	1.0155	1.0019	0.9824	1.013574209	1.019849349	212,64	29,26	120,1
SD7-3A	-0.394	1.048	113.79	1.0239	0.9828	0.9933	1.041819292	0.989429175	139,82	333,8	242,2
SD7-4A	-0.563	1.054	89.68	1.03	0.9904	0.9796	1.039983845	1.011024908	246,73	86,16	354,5
SD7-5A	-0.617	1.053	119.23	1.027	0.9879	0.9851	1.039578905	1.002842351	337,76	156,14	246,0
SD9-1A	0.243	1.023	26.57	1.0078	1.0006	0.9916	1.007195683	1.00907624	13,3	105,17	273,72
SD9-1B	0.648	1.086	13.28	1.03	1.0162	0.9538	1.013580004	1.06542252	189,39	52,42	299,23
SD10-1A	-0.329	1.221	1.94	1.1111	0.9755	0.9135	1.139005638	1.067870826	222,32	322,15	72,54
SD10-1B	-0.389	1.25	1.35	1.1263	0.9681	0.9057	1.163412871	1.068896986	200,58	17,32	108,1
SD10-2A	-0.869	1.031	4.92	1.0179	0.9919	0.9901	1.02621232	1.001817998	30,11	290,43	131,45
SD10-2B	0.147	1.057	5.54	1.0265	1.0025	0.971	1.02394015	1.032440783	213,13	89,67	308,19
SD10-3A	-0.44	1.274	1.04	1.1386	0.9614	0.9001	1.184314541	1.068103544	215,29	354,53	113,20
SD10-3B	-0.604	1.177	1.31	1.0944	0.9673	0.9383	1.131396671	1.030906959	222,21	45,69	313,1
SD11-1A	1	1.03	-7.48	-0.983	-1.0085	-1.0085	0.974714923	1	225,3	316,10	119,80
SD11-1B	-0.324	1.045	-6.53	-0.9895	-0.9951	-1.0243	0.994372425	0.971492727	29,0	119,80	299,10
SD11-2A	-0.212	1.078	-3.81	-0.9657	-0.9943	-1.04	0.971236045	0.956057692	199,2	106,58	291,32
SD11-2B	0.534	1.093	-3.64	-0.9506	-1.0146	-1.0348	0.936920954	0.98047932	37,63	270,17	174,20
SD11-3A	0.21	1.11	-2.31	-0.9453	-1.0064	-1.0484	0.939288553	0.959938955	62,53	234,37	327,4
SD11-3B	-0.863	1.113	-2.41	-0.9598	-0.9671	-1.0731	0.99245166	0.901220762	30,12	129,37	285,51
SD12-1A	-0.031	1.023	146.76	1.0117	0.9997	0.9885	1.012003601	1.011330298	56,11	165,59	320,28
SD12-2A	-0.212	1.04	87.06	1.0208	0.9971	0.9821	1.02376893	1.015273394	56,8	220,82	326,2
SD12-3A	-0.532	1.06	77	1.033	0.9899	0.9771	1.043539751	1.01309999	49,6	172,79	318,9
SD12-4A	-0.338	1.021	73.14	1.0116	0.9976	0.9908	1.014033681	1.006863141	258,12	146,59	354,28
SD12-5A	-0.373	1.018	83.29	1.0098	0.9978	0.9924	1.012026458	1.005441354	48,7	299,69	141,20
SD12-5B	-0.605	1.014	93.32	1.0078	0.9974	0.9948	1.01042711	1.002613591	43,15	217,75	312,2
SD12-5C	0.276	1.019	67.61	1.0087	1.0017	0.9896	1.00698812	1.012227162	227,7	326,50	132,39
SD13-1A	-0.745	1.013	116.06	1.0074	0.9971	0.9956	1.010329957	1.001506629	309,8	216,21	59,67
SD13-2A	-0.899	1.033	126.72	1.0187	0.9915	0.9899	1.027433182	1.001616325	315,3	223,29	51,61
SD13-2B	-0.27	1.021	118.81	1.011	0.9982	0.9909	1.012823082	1.00736704	311,20	220,2	124,70
SD13-3A	-0.013	1.016	109.79	1.0078	0.9999	0.9922	1.00790079	1.007760532	279,12	12,14	150,72
SD13-4A	-0.298	1.042	144.88	1.0224	0.9958	0.9817	1.026712191	1.01436284	274,14	4,2	103,76
SD13-5A	-0.269	1.033	137.18	1.0177	0.997	0.9853	1.020762287	1.011874556	299,11	209,2	110,79
SD14-1A	-0.301	1.094	7.15	1.0493	0.9905	0.9602	1.059363958	1.031555926	253,14	150,42	357,45
SD14-1B	-0.091	1.092	7.43	1.0455	0.9967	0.9578	1.048961573	1.040613907	269,1	178,42	0,48
SD14-2A	-0.957	1.115	6.34	1.064	0.969	0.967	1.098039216	1.002068252	234,25	336,24	103,54
SD14-2B	-1	1.048	6.93	1.0275	0.9863	0.9863	1.04177228	1	240,18	22,68	146,13
SD14-3A	-0.502	1.072	7.1	1.0394	0.9885	0.9722	1.05149216	1.016766098	256,1	166,22	347,68
SD14-3B	-0.733	1.108	7.16	1.0595	0.9763	0.9641	1.085219707	1.012654289	244,17	354,49	141,36
SD14-3C	-0.183	1.048	8.7	1.0248	0.997	0.9782	1.027883651	1.019218974	260,1	170,14	352,76
SD15-1A	0.468	1.023	-10.36	-0.9874	-1.0034	-1.0092	0.984054216	0.994252874	82,45	330,21	223,38
SD15-1B	0.005	1.02	-9.79	-0.9903	-1	-1.0097	0.9903	0.990393186	117,0	207,75	27,15
SD15-2A	-0.093	1.024	-8.39	-0.9886	-0.9992	-1.0122	0.989391513	0.987156688	41,38	231,52	135,5
SD15-3A	0.104	1.058	3.94	1.0271	1.0017	0.9713	1.025356893	1.03129826	86,34	190,20	306,49
SD15-3B	-0.364	1.067	3.97	1.0357	0.992	0.9723	1.044052419	1.020261236	273,49	69,39	169,12
SD15-4A	0.545	1.1	40.09	1.0372	1.0159	0.9468	1.020966631	1.072982678	323,18	55,6	162,71
SD15-4B	0.305	1.095	34.86	1.0407	1.0085	0.9508	1.031928607	1.060685738	332,22	241,3	142,68

Sample	T	P'	K	k1	k2	k3	k1/k2	k2/k3	kmax	kint	kmin
SD16-1A	-0.159	1.078	50.65	1.0395	0.9956	0.9649	1.044094014	1.031816769	239,7	147,22	346,67
SD16-1B	-0.11	1.077	57.92	1.0387	0.9968	0.9644	1.04203451	1.033596018	242,4	150,19	342,71
SD16-2A	-0.468	1.048	15.72	1.0263	0.9928	0.9809	1.033742949	1.012131716	243,4	345,72	152,17
SD16-2B	-0.334	1.05	19.23	1.0266	0.9945	0.9789	1.032277526	1.015936255	242,8	344,59	147,30
SD16-3A	-0.425	1.045	25.89	1.0248	0.9937	0.9815	1.031297172	1.012429954	241,9	147,25	351,63
SD16-3B	-0.378	1.03	58.77	1.0164	0.9963	0.9873	1.020174646	1.00911577	236,7	135,56	330,33
SD17-1A	-0.874	1.029	210.07	1.0168	0.9924	0.9908	1.02458686	1.001614857	118,15	211,9	331,72
SD17-1B	-0.587	1.032	166.81	1.0178	0.9941	0.998	1.02384066	0.996092184	124,13	218,18	0,67
SD17-2A	-0.518	1.028	181.09	1.0156	0.9954	0.9891	1.020293349	1.006369427	108,4	200,27	11,62
SD17-2B	0.038	1.025	163.83	1.012	1.0003	0.9877	1.011696491	1.01275691	120,7	214,31	18,58
SD17-3A	-0.155	1.02	214.68	1.0104	0.999	0.9907	1.011411411	1.008377915	126,5	220,42	31,48
SD17-3B	0.152	1.024	180.27	1.0113	1.0012	0.9875	1.010087895	1.013873418	129,14	234,46	27,41

Table 1. AMS results by site and specimen.

Sample	Room T x 10^-6	In liquid N x 10^-6	Low T meas./Room T. meas.
CO1-1A	107.573	100.683	0.93595
CO2-1A	177.345	147.848	0.833674
CO5-1B	112.735	147.44	1.307846
CO6-1A	41.502	23.063	0.555708
CO7-1B	38.315	117.364	3.063135
CO8-1A	120.309	44.027	0.365949
CO9-3A	183.828	162.927	0.886301
CO10-1A	120.852	72.14	0.596928
CO11-2A	110.19	82.291	0.74681
CO12-1B	22.199	37.43	1.686112
CO13-1B	235.78	117.786	0.499559
CO17-1A	216.956	208.761	0.962227
CO18-1A	306.138	187.999	0.614099
CO19-2A	38.83	40.939	1.054314
CO20-1A	23.401	43.425	1.85569
CO21-1A	181.871	201.591	1.108429
CO22-1A	29.172	24.099	0.8261
CO23-1A	37.968	51.27	1.350348
M1-2A	76.518	283.813	3.709101
SD2-1A	18.401	27.732	1.507092
SD3-1A	27.559	57.257	2.077615
SD4-1A	29.993	60.554	2.018938
SD6-1B	259.4	151.25	0.583076
SD7-1A	72.266	88.411	1.223411
SD8-1A	91.584	117.528	1.283281
SD9-1B	15.622	29.825	1.909167
SD12-1A	118.17	41.14	0.348143
SD13-1A	95.213	58.746	0.616996
SD16-1A	43.865	25.199	0.574467
SD17-1A	170.48	130.585	0.765984

Table 2. Low-T susceptibility measurements for problem-free samples.